Andriampenomanana, F., Nyblade, A. A., Wysession, M. E., Durrheim, R. J., Tilmann, F., Julià, J., Pratt, M. J., Rambolamanana, G., Aleqabi, G., Shore, P. J., Rakotondraibe, T. (2017): The structure of the crust and uppermost mantle beneath Madagascar. - *Geophysical Journal International*, *210*, 3, pp. 1525—1544.

DOI: http://doi.org/10.1093/gji/ggx243

Geophysical Journal International

Geophys. J. Int. (2017) **210,** 1525–1544
Advance Access publication 2017 June 3
GJI Seismology

doi: 10.1093/gji/ggx243

The structure of the crust and uppermost mantle beneath Madagascar

Fenitra Andriampenomanana,[1,2] Andrew A. Nyblade,[1,3] Michael E. Wysession,[4] Raymond J. Durrheim,[1] Frederik Tilmann,[5] Jordi Julià,[6] Martin J. Pratt,[4] Gérard Rambolamanana,[2] Ghassan Aleqabi,[4] Patrick J. Shore[4] and Tsiriandrimanana Rakotondraibe[1,2]

[1] *School of Geosciences, University of the Witwatersrand, Private Bag* 3 - 2050 *Wits, Johannesburg, South Africa. E-mail: nyonyfenitra@gmail.com*
[2] *Institut et Observatoire de Géophysique d'Antananarivo, Université d'Antananarivo, Ambohidempona - B.P* 3843, *Antananarivo* 101, *Madagascar*
[3] *Department of Geosciences, Penn State University,* 503 *Deike Building, University Park, PA* 16802, *USA*
[4] *Department of Earth and Planetary Sciences, Washington University in St. Louis, Campus Box* 1169, 1 *Brookings Dr, Saint Louis, MO* 63130-4899, *USA*
[5] *Deutsches GeoForschungsZentrum (GFZ), Telegrafenberg, D-*14473 *Potsdam, Germany*
[6] *Departamento de Geofisica & Programa de Pós-Graduação em Geodinâmica e Geofisica, Universidade Federal do Rio Grande do Norte, Natal, Brazil*

Accepted 2017 June 1. Received 2017 May 15; in original form 2016 November 12

SUMMARY

The lithosphere of Madagascar was initially amalgamated during the Pan-African events in the Neoproterozoic. It has subsequently been reshaped by extensional processes associated with the separation from Africa and India in the Jurassic and Cretaceous, respectively, and been subjected to several magmatic events in the late Cretaceous and the Cenozoic. In this study, the crust and uppermost mantle have been investigated to gain insights into the present-day structure and tectonic evolution of Madagascar. We analysed receiver functions, computed from data recorded on 37 broad-band seismic stations, using the H–κ stacking method and a joint inversion with Rayleigh-wave phase-velocity measurements. The thickness of the Malagasy crust ranges between 18 and 46 km. It is generally thick beneath the spine of mountains in the centre part (up to 46 km thick) and decreases in thickness towards the edges of the island. The shallowest Moho is found beneath the western sedimentary basins (18 km thick), which formed during both the Permo-Triassic Karro rifting in Gondwana and the Jurassic rifting of Madagascar from eastern Africa. The crust below the sedimentary basin thickens towards the north and east, reflecting the progressive development of the basins. In contrast, in the east there was no major rifting episode. Instead, the slight thinning of the crust along the east coast (31–36 km thick) may have been caused by crustal uplift and erosion when Madagascar moved over the Marion hotspot and India broke away from it. The parameters describing the crustal structure of Archean and Proterozoic terranes, including average thickness (40 km versus 35 km), Poisson's ratio (0.25 versus 0.26), average shear-wave velocity (both 3.7 km s^{-1}), and thickness of mafic lower crust (7 km versus 4 km), show weak evidence of secular variation. The uppermost mantle beneath Madagascar is generally characterized by shear-wave velocities typical of stable lithosphere (~4.5 km s^{-1}). However, markedly slow shear-wave velocities (4.2–4.3 km s^{-1}) are observed beneath the northern tip, central part and southwestern region of the island where the major Cenozoic volcanic provinces are located, implying the lithosphere has been significantly modified in these places.

Key words: Joint inversion; Sedimentary basin processes; Crustal structure.

1 INTRODUCTION

Madagascar displays a complex geological framework resulting from several tectonic events that span more than 2.5 billion years of Earth's history. The Malagasy lithosphere was originally amalgamated and reworked by the Neoproterozoic Pan-African Orogeny and later modified by a series of extensional events that lead to continental break-up from Africa in the Jurassic and from India during the Cretaceous (e.g. Rabinowitz *et al.* 1983; Coffin & Rabinowitz 1987; Collins 2006). In the Cenozoic, the tectonic evolution of Madagascar was marked by a series of magmatic events (e.g. Mahoney *et al.* 1991; Storey *et al.* 1995). Although Madagascar offers a unique geological framework to investigate how the continental crust is formed and then modified by extensional and

magmatic processes, little is known about its deep structure and composition.

In this paper, we contribute to the growing body of seismic constraints on crustal structure by investigating crustal structure across Madagascar. Teleseismic *P*-wave receiver functions have been used together with surface wave phase-velocity measurements to obtain 37 new point estimates of crustal thickness, shear-velocity structure, and Poisson's ratio spanning the island, along with estimates of uppermost mantle shear-wave velocity. These results were obtained using broadband seismic data recorded on both permanent and temporary seismic stations in Madagascar, modelled with two different methods, H–κ stacking of receiver functions (Zhu & Kanamori 2000) and a joint inversion of receiver functions and Rayleigh wave phase velocities (Julià *et al*. 2000, 2003). The temporary stations were part of two networks, the Madagascar-Comoros-Mozambique (MACOMO) network (Wysession *et al*. 2011), and the Seismological Signatures in the Lithosphere/Asthenosphere system of Southern Madagascar (SELASOMA) network (Tilmann *et al*. 2012). The ensemble of seismic stations enables us to examine crustal structure in each tectonic region of the island, and thus to gain insights into several processes that have formed and subsequently modified the crust and uppermost mantle beneath Madagascar.

Our findings shed new lights on the opening of rift basins and related thinning of the crust, the origin of high elevations across the island, crustal composition, secular variation in Precambrian crustal genesis, and geodynamic links between regions of low mantle seismic velocities and crustal structure. These results relate the different styles of separation from Africa and India to the different response of the crust, that is a large degree of crustal thinning is observed in the west related to the opening of the rift basins, whereas only very localized minor thinning is observed along the east coast following the separation from India. To first order, Archean and Proterozoic crust is observed to be similar. Low seismic velocities in the uppermost mantle beneath the northern, central, and southwestern parts of Madagascar are correlated with locations of Cenozoic volcanism.

2 TECTONIC SETTING

The geology of Madagascar can be divided into two major structural zones (Fig. 1). The western third of the island is covered by Late Carboniferous to Quaternary age sedimentary basins that consist of recent deposits lying on top of a Karoo sequence, while the remaining two-thirds of the island, on the eastern side, consist predominantly of Precambrian and Early Palaeozoic rocks that have been reworked during the Pan-African Orogeny (e.g. Nicollet 1990; de Wit 2003). Mesozoic and Cenozoic volcanic provinces are also found in several locations on the island (Fig. 1).

2.1 Sedimentary basins

The sedimentary basins along the western side of Madagascar formed during the separation of Madagascar from Africa, which started in the Late Paleaozoic and was complete by the Late Jurassic and Early Cretaceous (Rabinowitz *et al.* 1983; Piqué 1999a). During this separation, the East Gondwana Plate (Madagascar–India–Seychelles–Antarctica–Australia) moved south–southeasterly along a transform fault, which is currently known as the Davie Ridge (Segoufin & Patriat 1980; Coffin & Rabinowitz 1987; Cochran 1988; Piqué 1999a). A hotspot reconstruction places the southeastern region of Madagascar above the Marion hotspot during the Late Cretaceous (~90 Ma), which led to the separation of India–Seychelles from Madagascar (Storey *et al.* 1995; Torsvik *et al.* 1998; Piqué 1999a; Raval & Veeraswamy 2003). This separation was accompanied by significant magmatic activity along both the east and west coasts of Madagascar (Schlich 1975; Norton & Sclater 1979; Mahoney *et al.* 1991). Madagascar completely separated from India by the end of the Cretaceous (Dyment 1991).

While Madagascar was part of Gondwana, from the Carboniferous through the Early Triassic, Karoo sediments began accumulating in depressions that would eventually develop into the Antsiranana, Mahajanga and Morondava rift basins along the western part of the island (Fig. 1). The sedimentary rocks in these basins range in age from the Carboniferous to the present, with the basal formations consisting of Karoo sediments. The filling of the basins proceeded from south to north and from west to east, accompanying the northward progression of the opening of the basins (Besairie 1971; Piqué 1999a). Early studies of the western sedimentary basins of Madagascar suggested a sediment thickness of more than 10 km in the south, thinning out towards the north and east (Besairie 1971; Boast & Nairn 1982; Coffin & Rabinowitz 1988).

2.2 Precambrian basement

The Precambrian basement of Madagascar can be divided into six major units, approximately in order of decreasing age: Antongil-Masora craton, and the Antananarivo, Anosyen-Androyen, Ikalamavony, Vohibory and Bemarivo terranes (Fig. 1).

(1) *Palaeoarchean to Mesoarchean:* The Antongil-Masora craton is located along the east coast of Madagascar in two locations, the Antongil terrane in the mid-north and the Masora terrane in the mid-south. This craton contains the oldest rocks (~3.3 Ga) in Madagascar (Tucker *et al.* 2011) and is composed mainly of Palaeoarchean to Mesoarchean migmatic gneiss suites (Besairie 1968, 1969; Hottin 1976). It is usually interpreted as a fragment of the cratonic lithosphere of the Western Dharwar Craton in India (e.g. Raval & Veeraswamy 2003).

(2) *Neoarchean:* The Antananarivo terrane occupies the major portion of the Precambrian shield of Madagascar and its central high plateau. It is composed mostly of Neoarchean (~2.5 Ga) orthogneisses and paragneisses that grade from greenschist to granulite facies (Tucker *et al*. 2011, 2012).

(3) *Palaeoproterozoic:* The Anosyen-Androyen terrane constitutes the southernmost part of the Precambrian shield of Madagascar (Tucker *et al.* 2012). Geochronological data and common geological characteristics, such as a Palaeoproterozoic (~2.0–1.8 Ga) gneissic basement and sequences of Neoarchean and Palaeoproterozoic platform sediments, point to similarities between the Anosyen and Androyen subdomains, leading to their consideration as a single terrane.

(4) *Mesoproterozoic:* The Ikalamavony terrane forms a narrow NNW–SSE striking zone between the older Anosyen-Androyen and Antananarivo terranes. It is dominated by the Ikalamavony Group (~1.08–0.98 Ga), which includes higher-grade Mesoproterozoic metasedimentary and meta-igneous rocks (Cox *et al.* 2004; Tucker *et al.* 2007).

(5) *Neoproterozoic:* The Bemarivo terrane of northern Madagascar comprises Neoproterozoic (~758–708 Ma) intrusive granitic and volcanosedimentary rocks (Thomas *et al.* 2009; Tucker *et al.* 2012). The Vohibory terrane is located west of the Anosyen-Androyen terrane. It is an oceanic terrane of early Neoproterozoic

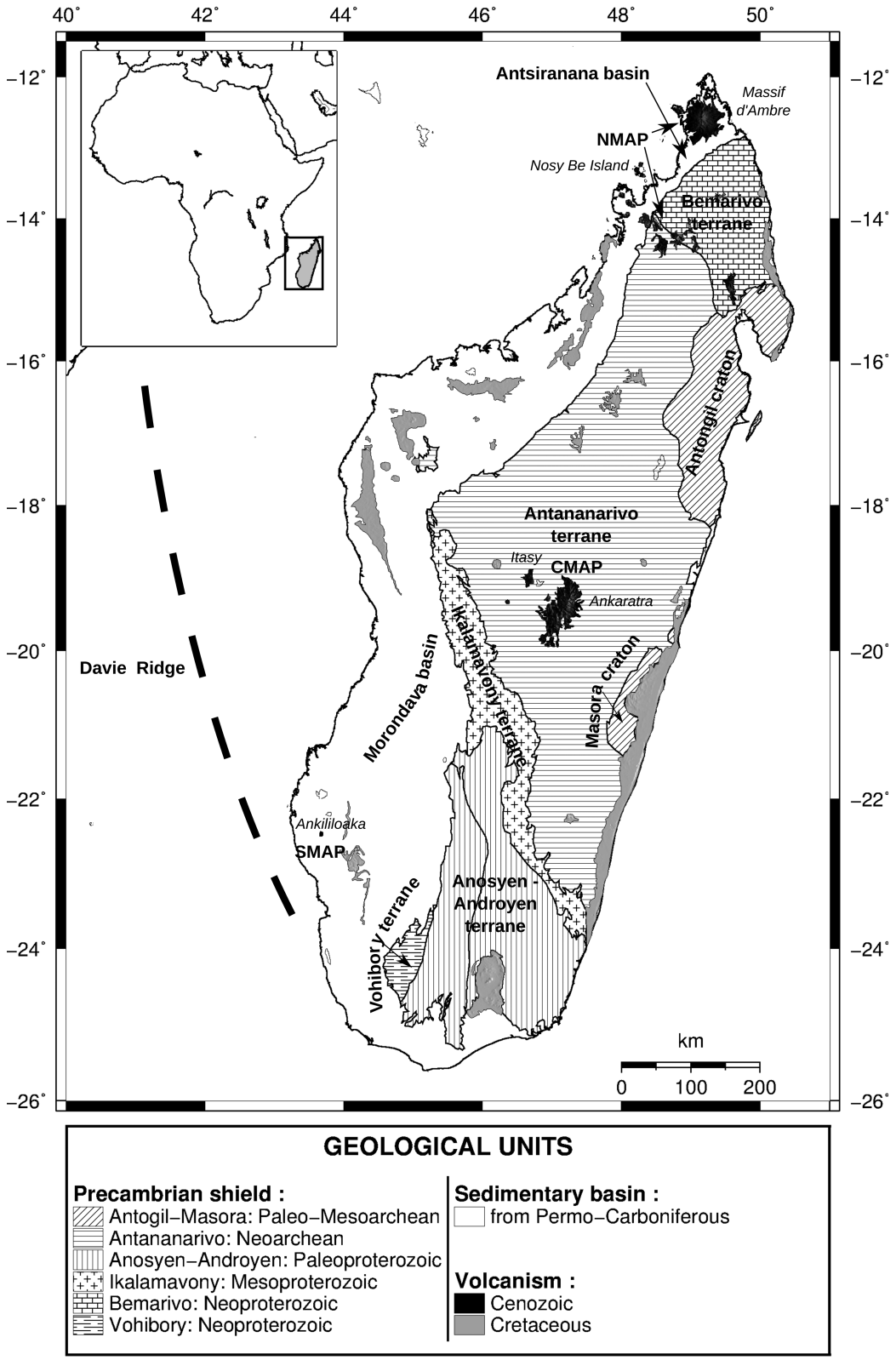

Figure 1. A simplified geological map of Madagascar showing the different geological units that are found in the study area (modified from Tucker *et al.* 2012) and locations of Cretaceous and Cenozoic volcanic provinces (NMAP/CMAP/SMAP).

age (~850 Ma), and is composed of intercalations of metabasalts, acidic volcanic rocks, and chemical metasedimentary rocks (GAF-BGR 2008; Jöns & Schenk 2008).

2.3 Volcanic provinces of Madagascar

Evidence of magmatism in Madagascar is characterized mainly by Cretaceous and Cenozoic eruptions (Besairie 1973). Intense fissural volcanism was associated with the dislocation of the East Gondwana Plate from the rest of Gondwana during the Permo-Triassic, as well as by the breaking apart of India, the Seychelles, Australia and Antarctica in the Cretaceous (~95–85 Ma) (Schlich 1975; Norton & Sclater 1979). As the latter volcanism coincided with the passage of Madagascar over the Marion hotspot, this resulted in the emplacement of mantle-derived tholeiitic basalts and crustal-derived dacite/alkali rhyolite magmas. Though these lavas may have once covered most of Madagascar, they are largely found today along the western, eastern and southern perimeter of the island (Storey *et al.* 1995; Torsvik *et al.* 1998).

Significant localized Cenozoic volcanic activity also occurred in several parts of Madagascar, as recently as the Quaternary (<1 Ma), such as in the Massif d'Ambre, Nosy Be Island, at the northern tip of Madagascar and in the Ankaratra and Itasy volcanic areas of the central highlands (Fig. 1). In general, Cretaceous volcanism was dominated by eruptions of tholeiitic basaltic lavas, while the Cenozoic volcanism primarily consisted of alkali basalt eruptions. A seismic analysis of the mantle roots of these volcanic terranes using surface waves revealed three large distinct seismic low-velocity regions that extend through the lithosphere and well into the asthenosphere beneath the northern (NMAP: Northern Madagascar Alkaline Province), central (CMAP: Central Madagascar Alkaline Province) and southwestern (SMAP: Southern Madagascar Alkaline Province) volcanic regions (Pratt *et al.* 2017; Fig. 1).

2.4 Previous studies of the crust of Madagascar

Although geological studies of Madagascar date back to the 1960s, very little is known about its deeper crustal structure. Previous studies have used local gravimetric data to model crustal thicknesses. Fourno & Roussel (1994) and Rakotondraompiana *et al.* (1999) reported a range of Moho depths from 25 to 40 km and 25 to 35 km, respectively. Rajaomazava (1992) used gravity data to model the crustal thickness beneath the Morondava basin and the central part of the island, reporting crustal thicknesses of 32–36 km and 32–38 km, respectively. Crustal thickness models for Africa, obtained from modelling satellite gravity data, show Madagascar Moho depths ranging between 35 and 42 km (Tedla *et al.* 2011; Tugume *et al.* 2013).

Because of a lack of seismic recording stations, there have been few seismological studies of the crust in Madagascar. Rakotondrainibe (1977) used traveltime analysis of body waves recorded at an array of short-period seismometers in the centre of Madagascar maintained by IOGA (Institut et Observatoire de Géophysique d'Antananarivo), and found a 36-km-thick crust beneath the central plateau. In the same region, Rambolamanana *et al.* (1997) used a simultaneous inversion of hypocentral parameters and crustal velocities to obtain a thickness of 42 km, and Rai *et al.* (2009) inferred a thickness of 38 km from receiver functions. A more recent study by Rindraharisaona *et al.* (2013), using a joint inversion of receiver functions and surface wave dispersion measurements from the four permanent broad-band seismic stations in Madagascar, found crustal thicknesses of 35 km beneath station SBV (in the north) and FOMA (in the south), 42 km beneath station ABPO (centre), and 39 km beneath station VOI (southcentral). The surface-wave tomography study of Pasyanos & Nyblade (2007) found crustal thicknesses in Madagascar to vary between 25 and 35 km, and the global CRUST 1.0 model shows crustal thicknesses ranging from 36 to 45 km (Laske *et al.* 2013). Recently, the crust in the southern part of Madagascar was investigated by Rindraharisaona *et al.* (2017) using the full SELASOMA data set, as well as data from additional stations in southern Madagascar. Using joint inversion of receiver functions and ambient-noise derived surface waves, they revealed a thinning of the crystalline crust to 13 km in the Morondava basin, and a slightly greater thickness of the Archean crust (~39 km) compared to the Proterozoic crust (~35 km). They also reported moderately thin crust (~30 km) along the eastern coast.

These studies suggest generally thick crust beneath the spine of mountains in the centre part of the island with a decrease in thickness towards the edges of the island, particularly towards the west. However, another study by Paul & Eakin (2017), from receiver function analysis beneath two permanents stations, suggested otherwise. In fact, they found that the central part of Madagascar is thinner (~39 km) than the eastern coast (~44 km). Additional information on crustal structure comes from a recent study of SKS splitting along the SELASOMA profile showing strong crustal anisotropy of up to 12 per cent in a 150 km broad zone located along the shear zones in southern Madagascar (Reiss *et al.* 2016).

3 DATA AND METHODS

3.1 Data

Most of the seismic data used in this study were collected from a recent deployment of 26 temporary broad-band seismic stations in Madagascar through the Madagascar–Comoros–Mozambique (MACOMO) project (Wysession *et al.* 2011; Fig. 2). Each seismic station was equipped with a 24-bit data logger (Quanterra Q330), a broad-band sensor (Guralp CMG-3T, Streckeisen STS-2, or Nanometrics Trillium 120PA), and a GPS clock. The data were recorded continuously at both 1 and 40 samples per second. These stations were deployed throughout the island between 2011 and 2013 in two parts: 10 seismic stations were installed mostly along the coasts in September, 2011. The remaining 16 stations were deployed in September, 2012, and all of the stations were removed from the field in August–September 2013.

In addition to MACOMO data, seismic data from five additional broad-band seismic stations were used: SKRH (AFRICAARRAY), ABPO (IRIS/GSN), FOMA (GEOSCOPE) and VOI and SBV (GEOFON). A further seven seismic stations were used from the SELASOMA experiment (Tilmann *et al.* 2012), which included a linear deployment of temporary broad-band seismic stations across the southern part of Madagascar (Fig. 2). In summary, a total of 37 temporary and permanent seismic stations were used in this study (listed in Table S1). Rayleigh wave phase-velocity measurements derived from ambient-noise analysis and teleseismic surface wave tomography have been taken from Pratt *et al.* (2017).

3.2 Receiver functions

Receiver functions are time series composed of *P*-to-*S* converted phases generated after the interaction of a

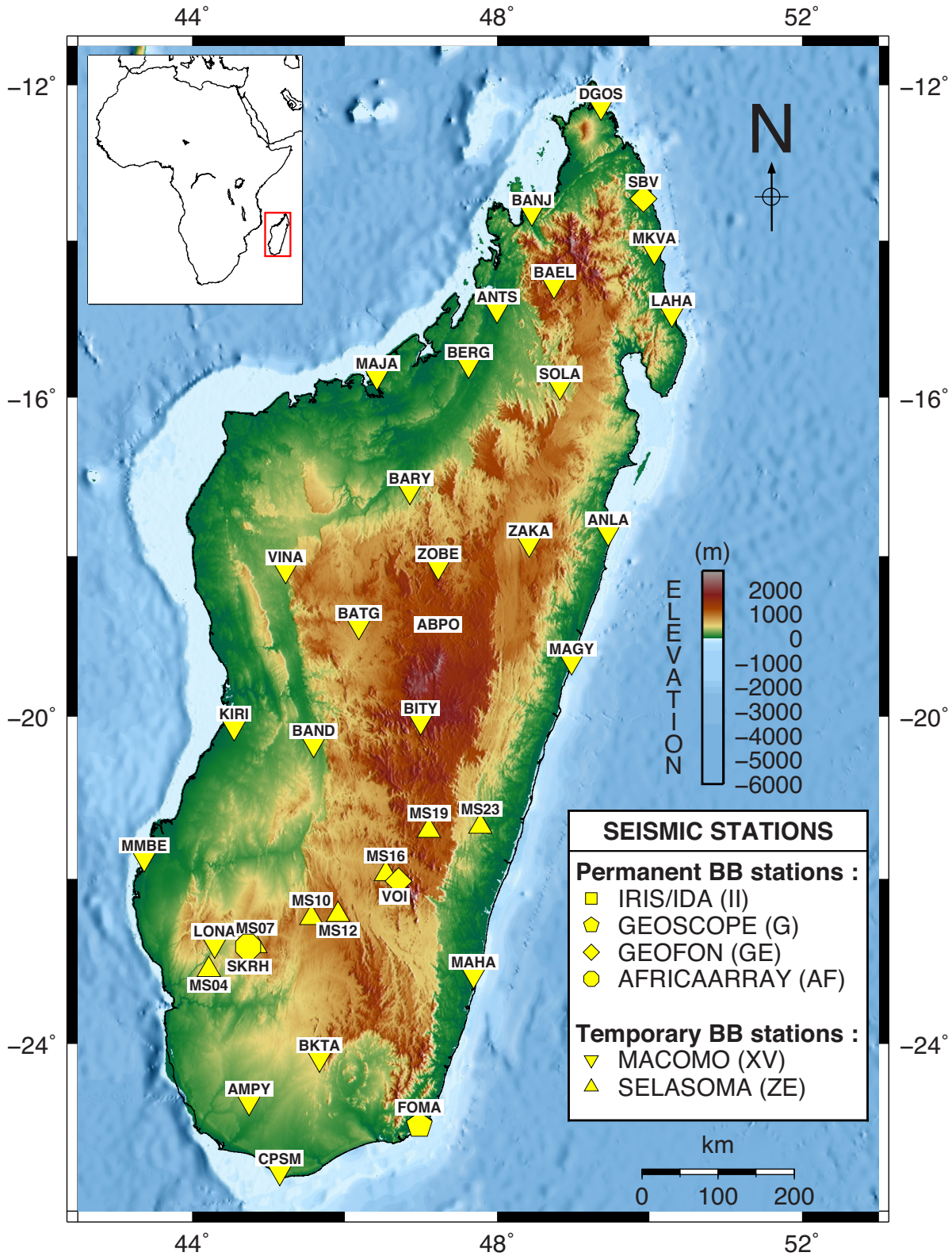

Figure 2. Topographic map of Madagascar showing the distribution of temporary and permanent seismic stations used in this study.

teleseismic *P*-wave front with subsurface discontinuities local to the recording station (Fig. 3). The main phases include the *P*-to-*S* conversion upon refraction (Ps) and the multiple reverberations between the free-surface and the discontinuity (PpPs and PsPs+PpSs). The time and amplitude of the *P*-to-*S* conversions are mainly controlled by the *S*-velocity contrasts and the corresponding *S*-*P* traveltimes, and are commonly utilized to determine the *S*-velocity structure under the recording sites (Langston 1979; Owens *et al.* 1984; Ammon *et al.* 1990; Cassidy 1992).

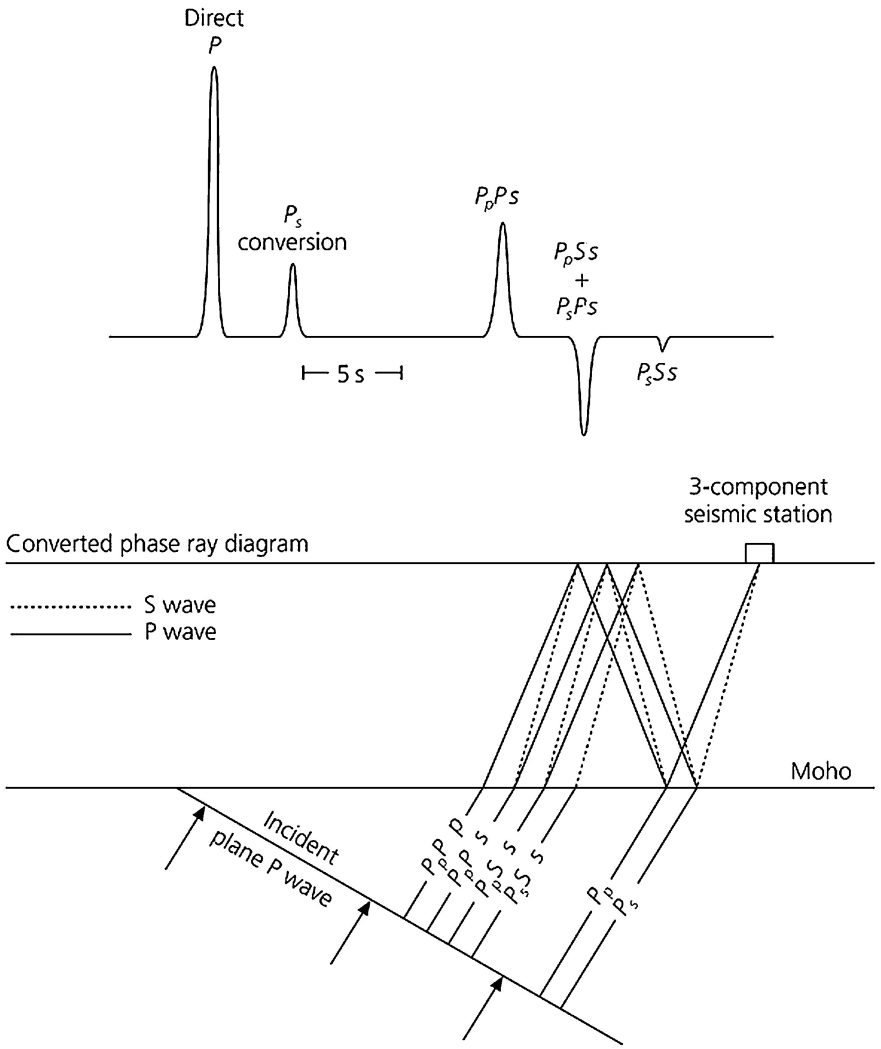

Figure 3. Top panel: synthetic radial receiver function waveform. Bottom panel: corresponding seismic ray diagram of *P*-to-*S* converted phases that contain the receiver function of a single layer over a half-space (taken from Stein & Wysession 2003).

A total of 143 teleseismic events with moment magnitude $M_w \geq 5.5$ and epicentral distances between 30° and 95° were used to compute radial and tangential receiver functions through the iterative time-domain deconvolution procedure of Ligorría & Ammon (1999) (Fig. 4 and listed in Table S2). The original waveforms were windowed 10 s before and 100 s after the *P*-wave arrival, de-trended, tapered and band-pass filtered between 0.05 Hz (to remove low-frequency noise) and 4 Hz (to avoid aliasing), before decimation to 10 samples per second. Horizontal components were then rotated along the great-circle path into radial and transverse components. Finally, *P*-wave radial and tangential receiver functions were obtained by deconvolving the vertical component from the corresponding radial and tangential components. Receiver functions were computed at two overlapping frequency bands with corner frequencies of 0.5 and 1.25 Hz, corresponding to Gaussian filter widths of 1.0 and 2.5, respectively. Receiver function amplitudes are frequency-dependent when second-order discontinuities are present under the station, so the use of overlapping frequency bands helps to discriminate sharp discontinuities from gradational transitions (Julià 2007).

To assess the quality of the receiver functions, each radial receiver function was convolved with its corresponding observed vertical-component seismogram to reconstruct the radial-component seismogram, and only radial receiver functions that recovered ≥85 per cent of the observed radial-component seismogram were selected for further analysis (Ligorría & Ammon 1999). In addition, data from events with large tangential receiver functions were discarded. Tangential receiver functions can be used to estimate the degree of heterogeneity and anisotropy of the propagating medium (Cassidy 1992), with small amplitudes on the tangential receiver functions indicating a predominantly 1-D and isotropic medium beneath a receiver. Fig. 5 shows examples of radial receiver functions computed for a Gaussian filter width of 1.0 for a permanent and a temporary seismic station, ABPO and ZAKA, respectively. Receiver functions for all stations are given in Fig. S1.

3.3 *H–κ* stacking method

The *H–κ* stacking method developed by Zhu & Kanamori (2000) was used to estimate crustal thickness (*H*) and *Vp*/*Vs* ratio (*κ*) beneath each station using receiver functions that have clear Ps waves and one or more multiple reverberations (PpPs, PsPs +PpSs, PsSs). The technique applies a grid search through *H* and *κ* parameter

Figure 4. Distribution of earthquakes (black dots) centred on the middle of the seismic network (black star). The two grey lines indicate the minimum (30°) and maximum (95°) event-station distances, in degrees, used in the receiver-function computations.

space that stacks the receiver function amplitudes along the corresponding phase-moveout curves according to

$$s(H,\kappa) = \sum_{j=1}^{N} w_1\, r_1\,(t_1) + w_2 r_2\,(t_2) - w_3 r_3\,(t_3)\,, \qquad (1)$$

where w_1, w_2 and w_3 are *a priori* weights assigned to the Ps, PpPs and PsPs+PpSs phases, respectively; r_j is the amplitude of the radial receiver function; t_1, t_2 and t_3 are the arrival times of the phases, and N is the number of receiver functions used. The best estimates of H and κ correspond to a maximum of the $s(H,\kappa)$ surface, which in turn matches the arrival times of the Ps, PpPs and PsPs+PpSs phases. The stacking procedure requires the assumption of an average Vp for the crust, which was fixed at the continental average of 6.5 km s^{-1} (e.g. Christensen & Mooney 1995).

When applying the stacking procedure to the data set, weights for the Ps, PpPs and PsPs+PpSs phases are usually selected depending upon the clarity of the phases. When all three phases were distinctly seen in the receiver-function waveforms, weighting factors of $w_1 = 0.4$, $w_2 = 0.3$ and $w_3 = 0.3$ were chosen. However, when the PpPs and PsPs+PpSs phases were less clear than the Ps phase, a higher weight of 0.6 was given to the Ps phase, and smaller but equal weights of 0.2 to the PpPs and PsPs+PpSs phases. Receiver functions computed with a Gaussian filter width of 1.0 were used for most of the stations, and receiver functions computed with a Gaussian filter width of 2.5 were used to check for consistency. However, for stations ABPO, MAHA, MS10, MS12, MS16, SBV and VOI the Ps and converted phases on the receiver functions computed using a Gaussian filter width of 2.5 were more easily identified, and therefore the results reported for these stations are from the H–κ stacking of the higher-frequency receiver functions. In addition, in sedimentary basins, reverberations from the sediment-basement interface can make the Ps and Moho reverberations difficult to identify, so the H–κ stacking technique was not used for some of the seismic stations in the sedimentary basins.

The approach of Julià & Mejía (2004) was used to estimate the uncertainty in the results from the H–κ stacking method. This approach employs a bootstrap resampling technique (Efron & Tibshirani 1991) to compute a one-standard-deviation error around the best-estimated values of H and κ. This involved resampling the receiver-function data sets with replacement 200 times for each station, applying the H–κ stacking procedure to the resampled data set, and computing the average and standard deviations from the resulting 200 estimates. In addition, to evaluate uncertainties

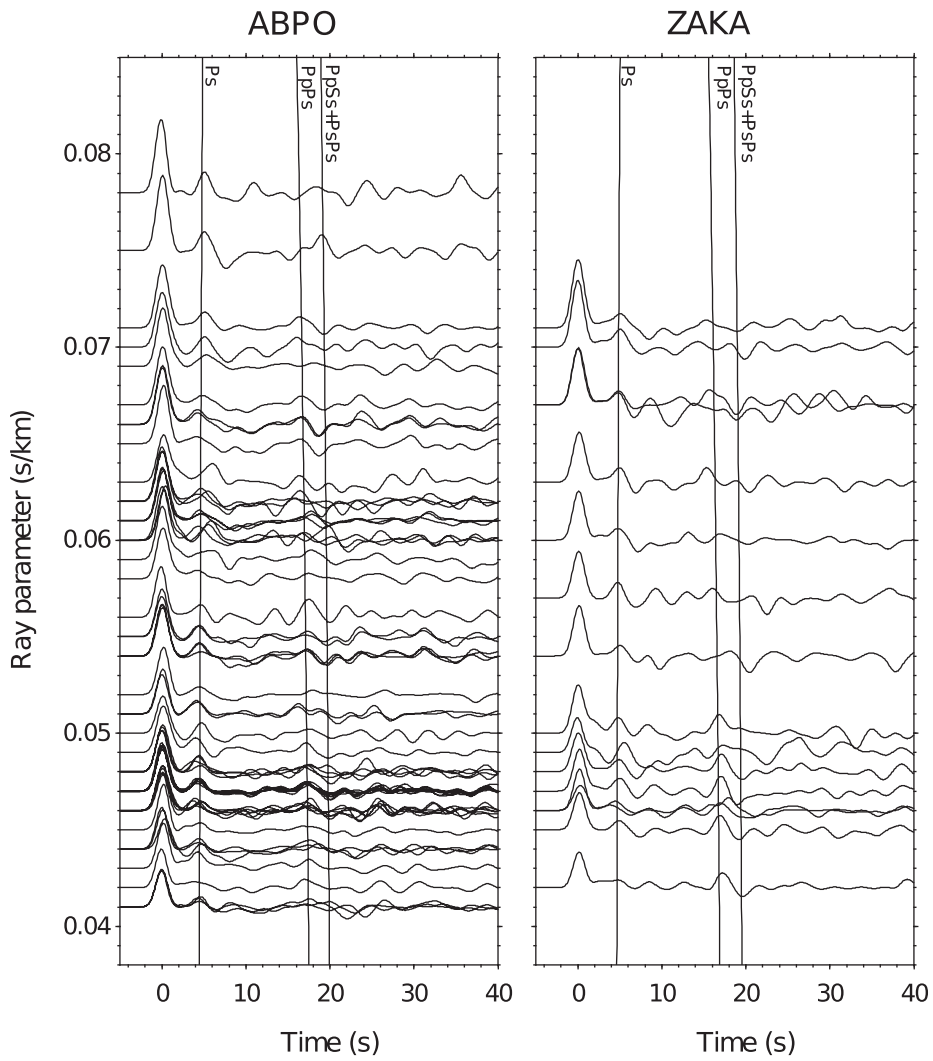

Figure 5. A plot of the radial receiver functions from a permanent seismic station, ABPO (left-hand panel), and a temporary station, ZAKA (right-hand panel), versus ray parameters estimated using a Gaussian filter width of 1.0. The three vertical lines show the predicted Ps, PpPs and PsPs+PpSs phase arrival times.

resulting from the choice of an average crustal *Vp*, the stacking procedure was applied using a range of *Vp* between 6.3 and 6.8 km s^{-1}. Overall uncertainties in H and κ were obtained by combining the formal uncertainties from the bootstrap method with the range of H and κ values obtained when using different *Vp* values. The overall uncertainties for each station are ±1–3 km for the Moho depth and ±0.02 for κ. An example of H–κ stacking for station VINA is shown in Fig. 6, and the results for all stations using an average crustal *Vp* of 6.5 km s^{-1} are summarized in Tables 1 and 2 and given in Fig. S2.

3.4 Joint inversion of receiver functions with the dispersion of Rayleigh wave phase velocities

For obtaining estimates of crustal thickness and crustal shear-wave velocities, the method developed by Julià *et al.* (2000, 2003) was used, which involves jointly inverting the receiver functions and surface-wave dispersion curves using an iterative, least-squares algorithm with a roughness norm. The input for the joint inversion consists of an initial velocity model, the observed receiver functions, and the Rayleigh-wave phase-velocity curves. An influence factor is used to control the trade-off between fitting the receiver functions and the phase-velocity dispersion curves, and equal contributions of receiver functions and dispersion data were used. Velocity models are parameterized as a stack of thin layers of fixed thickness and uniform velocity, so a smoothness parameter is needed to regularize the inversion by controlling the trade-off between fitting the observations and smoothing the velocity model. Rayleigh-wave phase velocities from 8 to 100 s, taken from the surface-wave tomography studies of Madagascar by Pratt *et al.* (2017), were used after applying a 3-point running average to smooth the dispersion curve.

The starting model used in the joint inversions consisted of an isotropic medium with a 35.5-km-thick crust and a linear shear-wave-velocity increase across the crust of 3.4–4.0 km s^{-1}, overlying a flattened PREM (Preliminary Reference Earth Model) structure for the mantle (Dziewonski & Anderson 1981). The crustal Poisson's ratio was set to the value obtained from the H–κ stacking at each station and crustal densities were obtained from the values of *Vp* using the empirical relationship of Berteussen (1977). The preset thicknesses of the first and second layers were, respectively, 1 and 2 km, and the layer thickness increased to 2.5 km for depths between 3 and 60.5 km, 5 km for depths between 60.5 and 260.5 km, and 10 km below 260.5 km depth. The velocity structure from the inversion is fixed to the PREM-like values for depths below 200 km.

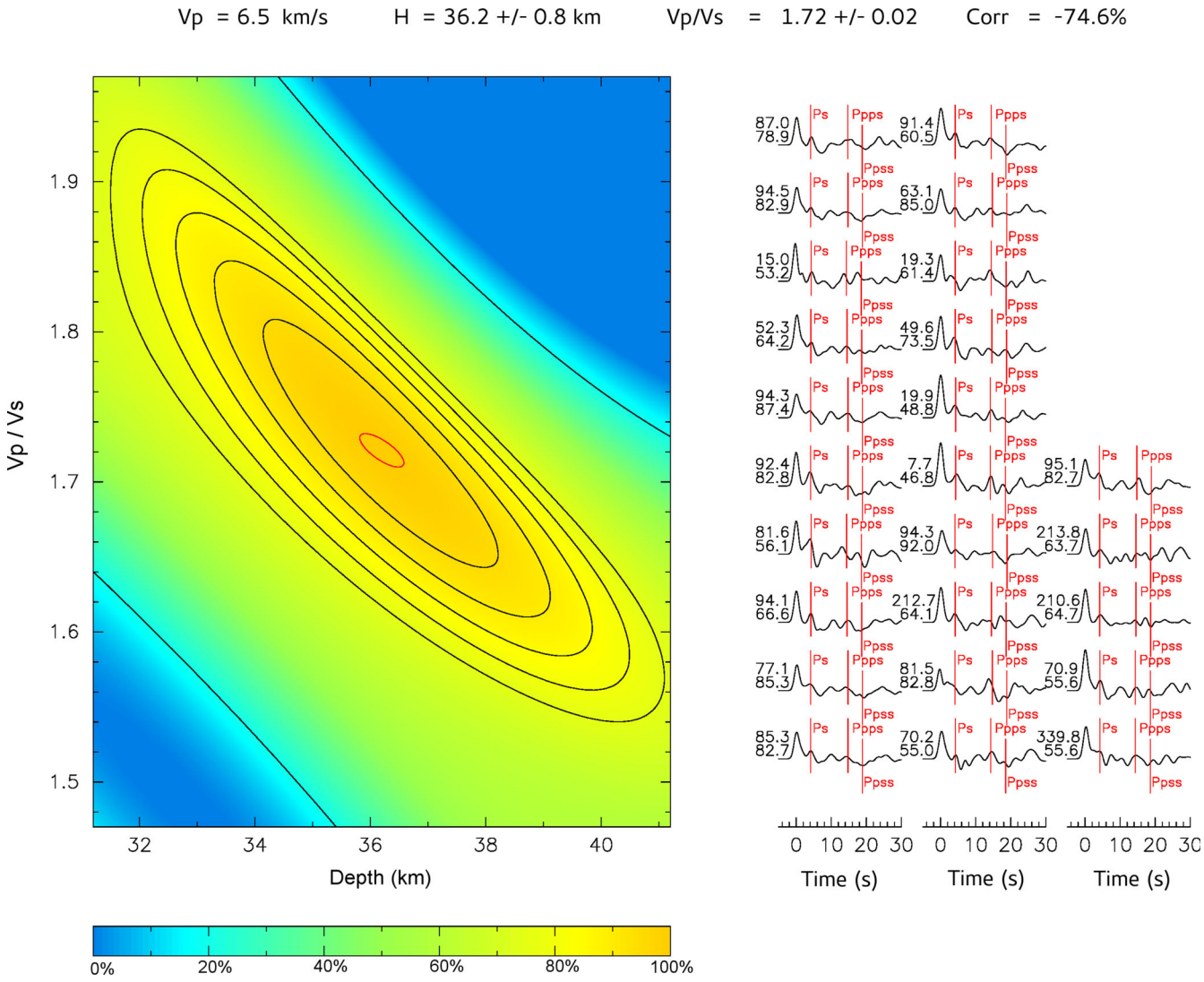

Figure 6. *H–κ* stacking results for seismic station VINA. Left-hand panel: *H–κ* parameter space with the optimal values for *H* and *κ* (centre of red ellipse). The black contours map out the percentage values, in the colour scale bar, of the normalized objective function given in eq. (1). Right-hand panel: receiver functions labelled by the event backazimuth (top number) and epicentral distance (bottom number), both in degrees. The optimal results for *H* and *κ* obtained are summarized along the top, along with their formal uncertainties, and shown with the red contour on the left panel.

The starting model for the seismic stations installed in the sedimentary basins was slightly different. The top 10 km of the sedimentary basin was characterized by a linear shear-wave velocity structure increasing from 2.2 to 3.6 km s^{-1} with a layer thickness of 1 km. Poisson's ratio was set to 0.35 for the top 3 km and then 0.29 for the remaining 7 km. Again, the densities were determined using the velocity–density relationship from Berteussen (1977).

The radial receiver functions were grouped by backazimuth and ray parameter before the joint inversion to account for laterally varying structures (Julià *et al.* 2008). Both high- and low-frequency receiver functions were binned into groups in which bounds in backazimuth and ray parameter were limited to maximum variations of 10° and 0.01 s km^{-1}, respectively. A minimum of three receiver functions was required to compute an average. Inversion results for each group yielded similar velocity structures for each station, indicating minimal lateral variations in crustal structure below each station. Consequently, all of the groups of receiver functions were inverted together to obtain an average velocity model for each station. An example of the joint inversion for station VINA is shown in Fig. 7, with the crustal structure for all stations summarized in Tables 1 and 2. The inversion results for the other stations are provided in Fig. S3.

Uncertainties in the velocity models were estimated by applying the approach of Julià *et al.* (2005) of repeating the inversion for a range of inversion parameters and Poisson's ratios. Doing this, we estimate an uncertainty of approximately 0.1 km s^{-1} for the velocity in each layer, which translates into an uncertainty of ±2.5 km in the depth of any crustal boundary observed in the model, including the Moho.

4 RESULTS

A correlation of *H–κ* stacking (for basement stations) with the joint inversion results shows a generally comparable estimation of crustal thickness for all seismic stations (Fig. 8). Consequently, only results from the joint inversion method are used to summarize the results for

Table 1. Summary of crustal structure parameters for stations located in the sedimentary basins along the western side of Madagascar.

Station name	Network code	#Events	*H–κ* stacking		Joint inversion					
			Crustal thickness (km)	Poisson's ratio	Sediment thickness (km)	Average sediment *Vs* (km s^{-1})	Crustal thickness (km)	Average crustal *Vs* (km s^{-1})	Average uppermost mantle *Vs* (km s^{-1})	Mafic lower crust (km)
DGOS	XV	34	–	–	4	2.3	18.0	3	4.3	0.0
BANJ	XV	13	–	–	4	2.4	33.0	3.5	4.3	12.5
ANTS	XV	22	28.6 ± 0.9	0.29 ± 0.02	6	2.7	33.0	3.4	4.4	5.0
BERG	XV	20	30.1 ± 1.3	0.31 ± 0.01	2	2.4	35.5	3.5	4.5	5.0
MAJA	XV	34	–	–	6	2.2	35.5	3.4	4.3	2.5
BAND	XV	17	33.6 ± 1.7	0.26 ± 0.03	2	2.6	33.0	3.4	4.3	2.5
KIRI	XV	19	–	–	6	2.7	28.0	3.3	4.3	2.5
MMBE	XV	10	–	–	8	2.1	23.0	2.8	4.4	2.5
MS07	ZE	13	26.9 ± 2.4	0.31 ± 0.04	6	2.8	30.5	3.3	4.4	5.0
SKRH	AF	8	–	–	5	2.7	28.0	3.2	4.4	0.0
LONA	XV	30	–	–	5	2.3	28.0	3.2	4.3	0.0
MS04	XV	13	–	–	5	2.3	25.5	3.2	4.4	2.5
CPSM	XV	34	28.0 ± 1.0	0.28 ± 002	0	0.0	33.0	3.6	4.5	5.0
Average ± standard deviation			**29.4 ± 2.6**	**0.29 ± 0.02**	**4.5 ± 2.1**	**2.3 ± 0.7**	**29.5 ± 5.2**	**3.3 ± 0.2**	**4.4 ± 0.1**	**3.5 ± 3.3**

Note the crustal thickness and average properties represent the total crust, that is sedimentary layers plus crystalline basement.

Table 2. Summary of crustal structure parameters for stations located within Precambrian terranes.

Terrane (age)	Station name	Net. code	#Events	*H–κ* stacking		Joint inversion			
				Crustal thickness (km)	Poisson's ratio	Crustal thickness (km)	Average crustal *Vs* (km s^{-1})	Average uppermost mantle *Vs* (km s^{-1})	Mafic lower crust (km)
Antongil-Masora (Palaeoarchean to Mesoarchean)	ANLA	XV	24	43.5 ± 1.4	0.24 ± 0.02	43.0	3.7	4.5	15.0
	BAEL	XV	24	33.5 ± 0.9	0.27 ± 0.02	33.0	3.7	4.4	2.5
	SOLA	XV	9	33.0 ± 1.2	0.24 ± 0.02	33.0	3.6	4.3	2.5
	BARY	XV	10	40.0 ± 2.5	0.25 ± 0.03	40.5	3.7	4.5	5.0
	ZAKA	XV	16	41.4 ± 1.7	0.25 ± 0.01	43.0	3.7	4.4	2.5
	ZOBE	XV	13	46.3 ± 2.1	0.22 ± 0.04	45.5	3.8	4.3	17.5
Antananarivo	BATG	XV	12	42.3 ± 1.4	0.27 ± 0.02	43.0	3.7	4.3	7.5
(Neoarchean)	ABPO	II	59	43.9 ± 1.2*	0.22 ± 0.01*	43.0	3.7	4.3	5.0
	MAGY	XV	14	28.9 ± 1.9	0.28 ± 0.04	35.5	3.7	4.3	5.0
	BITY	XV	14	41.6 ± 2.4	0.26 ± 0.02	43.0	3.7	4.3	10.0
	MS19	ZE	15	40.8 ± 1.3	0.27 ± 0.01	40.5	3.7	4.4	2.5
	MS23	ZE	20	41.6 ± 2.9	0.26 ± 0.02	40.5	3.8	4.5	7.5
	MAHA	XV	14	35.9 ± 0.9*	0.28 ± 0.01*	35.5	3.7	4.4	5.0
	VOI	GE	8	43.1 ± 2.4*	0.22 ± 0.04*	40.5	3.7	4.5	4.5
Average ± standard deviation				**39.4 ± 5.0**	**0.25 ± 0.02**	**39.7 ± 4.1**	**3.7 ± 0.0**	**4.4 ± 0.1**	**5.9 ± 4.2**
	MS12	ZE	9	39.1 ± 1.4*	0.24 ± 0.02*	38.0	3.7	4.5	5.0
Anosyen-Androyen	BKTA	XV	11	39.5 ± 1.1	0.21 ± 0.02	38.0	3.7	4.5	5.0
(Palaeoproterozoic)	MS10	ZE	11	36.2 ± 1.1*	0.27 ± 0.02*	35.5	3.6	4.5	2.5
	FOMA	G	24	36.5 ± 1.6	0.25 ± 0.03	35.5	3.7	4.4	5.0
Average ± standard deviation				**37.8 ± 1.7**	**0.24 ± 0.03**	**36.8 ± 1.4**	**3.7 ± 0.1**	**4.5 ± 0.0**	**4.4 ± 1.3**
Ikalamavony	VINA	XV	24	36.2 ± 0.8	0.24 ± 0.01	35.5	3.6	4.4	5.0
(Mesoproterozoic)	MS16	ZE	17	41.6 ± 0.8*	0.23 ± 0.01*	40.5	3.7	4.5	7.5
Average ± standard deviation				**38.9 ± 3.8**	**0.24 ± 0.01**	**38.0 ± 3.5**	**3.7 ± 0.1**	**4.5 ± 0.1**	**6.3 ± 1.8**
Bemarivo (Neoproterozoic)	SBV	GE	20	31.1 ± 1.8*	0.25 ± 0.03*	30.5	3.6	4.2	2.5
	MKVA	XV	10	31.3 ± 1.2	0.33 ± 0.01	35.5	3.7	4.3	2.5
	LAHA	XV	26	31.1 ± 1.1	0.31 ± 0.01	33.0	3.7	4.3	0.0
Average ± standard deviation				**31.2 ± 0.1**	**0.30 ± 0.04**	**33.0 ± 2.5**	**3.7 ± 0.1**	**4.3 ± 0.1**	**1.7 ± 1.4**
Vohibory (Neoproterozoic)	AMPY	XV	7	25.5 ± 2.4	0.30 ± 0.03	28.0	3.5	4.4	0.0

*Results obtained from receiver functions computed using a Gaussian filter width of 2.5.

Moho depth. Moreover, this technique was applied for all seismic stations (37 stations) while the *H–κ* stacking could only be applied for stations located in the basement and a few in the basin (29 stations in total). Results from *H–κ* stacking and the joint inversion of receiver functions and Rayleigh-wave phase-velocity dispersion measurements are summarized in Tables 1 and 2 and illustrated in Figs 9–13.

2-D contour maps were generated by interpolating the point measurements from the *H–κ* stacking and the joint inversion methods using the surface routine of the Generic Mapping Tools (GMT;

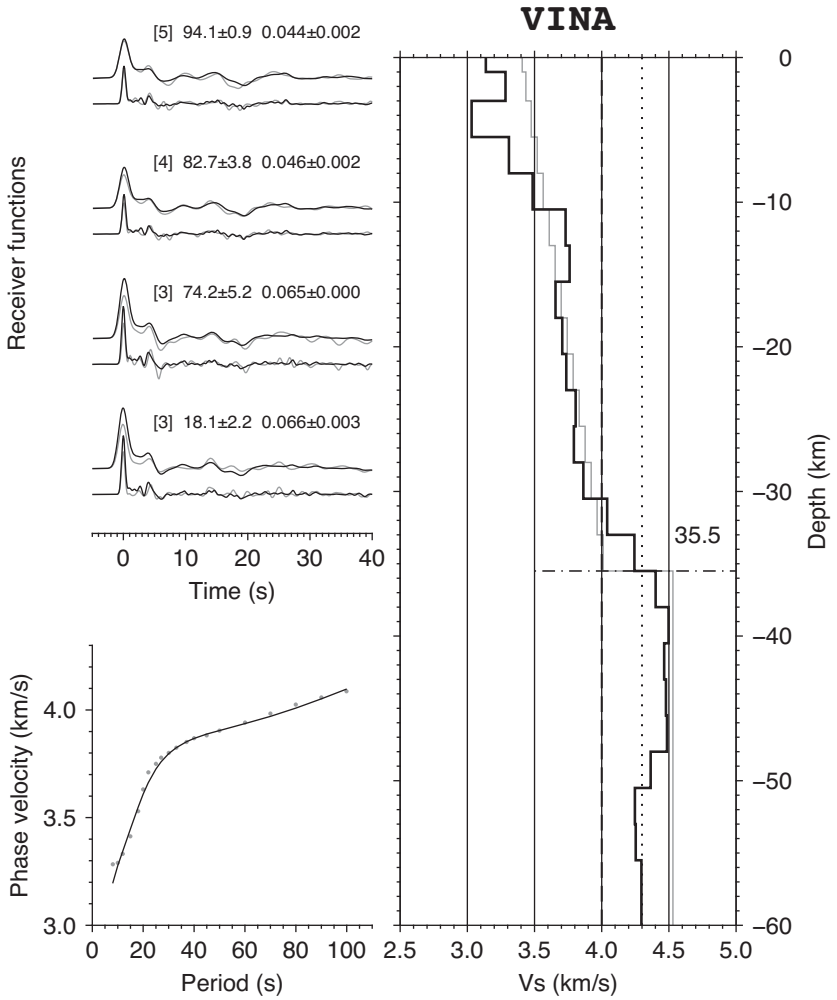

Figure 7. Joint inversion of Rayleigh wave phase velocities and receiver functions for station VINA. Top left-hand panel: grey and black lines are the observed and predicted radial receiver functions, respectively, estimated for Gaussian filter widths of 1.0 (top panel) and 2.5 (bottom panel). The numbers on top of the waveforms are the number of receiver functions stacked (in the square bracket), the average back azimuth (± one standard deviation), and the average ray parameter (±1 standard deviation) for the stack. Bottom left-hand panel: the observed and predicted dispersion curves of the phase velocity, shown with grey dots and a black line, respectively. Right-hand panel: the starting velocity model (grey line) and predicted velocity structure (black line). The horizontal dash-dot line and number indicate the Moho depth (in km). The vertical dashed and dotted lines correspond to *Vs* values of 4.0 and 4.3 km s^{-1}.

Wessel & Smith 1998). Only interpolated values within a 1°-radius distance from the point measurements are shown in the maps. Fig. 9 shows the sediment thickness from joint inversion, and Figs 10 and 11 show the Moho depth and Poisson ratio or average crustal *Vs* derived from *H–κ* stacking and joint inversion, respectively. Fig. 12 shows topography and crustal thickness along a south-to-north profile across Madagascar. Fig. 13 shows the correlation of the shear-wave velocity distribution in the uppermost mantle from the surface-wave tomography of Pratt *et al.* (2017) with that obtained from the joint inversion technique in this study.

A number of the parameters provided in Tables 1 and 2 have been interpreted from the shear-wave velocity profiles. Previous studies (e.g. Holbrook *et al.* 1992; Christensen & Mooney 1995; Rudnick & Fountain 1995; Rudnick & Gao 2003) have shown that lower crustal mafic lithologies such as amphibolites, garnet-bearing and garnet-free mafic granulites, and mafic gneisses typically have shear-wave velocities that are higher than 3.9 km s^{-1}. Therefore, to determine the thickness of the mafic lower crust we use the thickness of layers in the lowermost crust with velocities between 4.0 and 4.3 km s^{-1}. The depth where the shear-wave velocity is ≥4.3 km s^{-1} is taken as the Moho. For most stations, at this depth there is also a recognizable step increase or discontinuity in the shear-wave velocity.

Previous studies have shown that typical shear-wave velocities in sedimentary rocks are less than 3.0 km s^{-1} (e.g. Castagna *et al.* 1985; Brocher 2005). Therefore, the combined thickness of the layers with shear-wave velocity lower than 3.0 km s^{-1} were used as an estimate of the thickness of the sedimentary basin in the western region of Madagascar.

4.1 Sedimentary basins

Thirteen seismic stations (ANTS, BAND, BANJ, BERG, CPSM, DGOS, KIRI, LONA, MAJA, MMBE, MS04, MS07 and SKRH) are located in the western sedimentary basins. Our results show that the thickest sedimentary sections are observed beneath the western parts of the basins: about 6–8 km along the west coast beneath the Morondava and Mahajanga basins, thinning out rapidly eastward to only 2 km near the eastern edge of the basin. A variation in maximum sediment layer thickness is also observed along the north-south direction, from 5 to 8 km in the south to 4 km in the north.

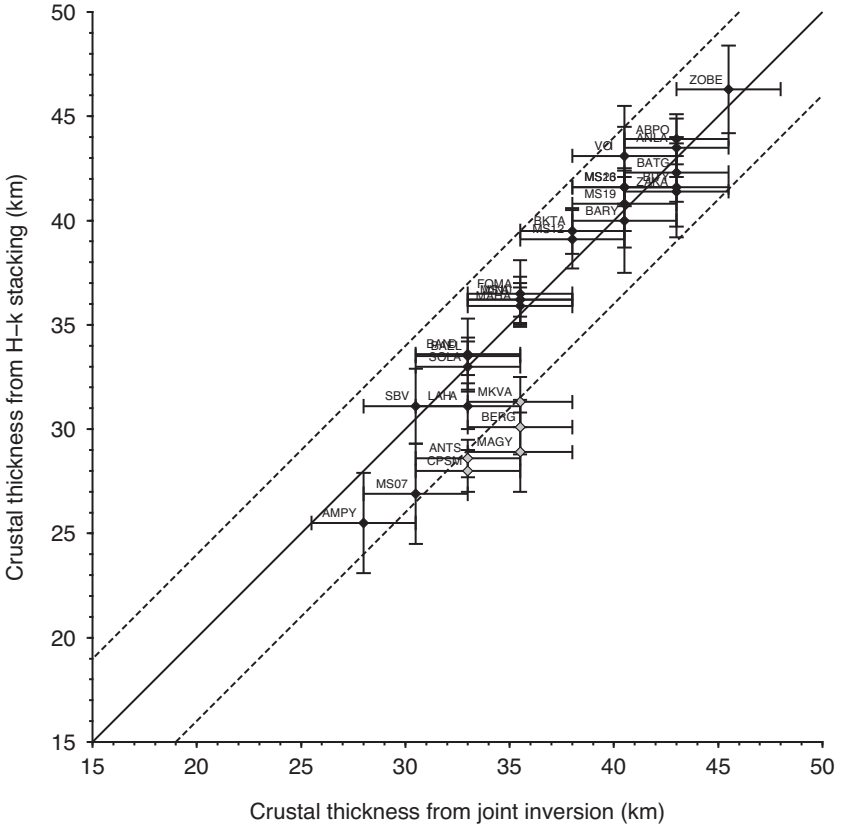

Figure 8. Crustal thickness values estimated from *H–κ* stacking techniques versus the joint-inversion method. The solid line indicates a one-to-one correlation between the two estimates and the dashed lines show a difference of ±4 km. Stations represented in grey are outside of the ±4 km zone and are either from stations in the sedimentary basins where crustal thickness is more difficult to constrain because of reverberations from the sediment-basement interface (BERG), or stations that generally present a gradational Moho in the velocity structure (CPSM, ANTS, MAGY and BERG).

The shear-wave velocities of the sedimentary layers range from 2.1 to 2.7 km s^{-1} in the western regions of the basins, with an average of 2.3 km s^{-1}, and from 2.4 to 2.8 km s^{-1} in the eastern regions, with an average of 2.6 km s^{-1}.

The basins are also characterized by a thin crust, with the Moho at depths between 18 and 36 km under the stations in the sedimentary basin, with an average of 30 ± 5 km. The total crustal thickness, i.e. sediments and basement, ranges from 23 to 33 km in the central and western parts of the basins and between 31 and 36 km in the eastern part of the basins. The northernmost part of the basin region has the thinnest crust, characterized by a Moho at 18 km depth. The crust is also characterized by slow average shear-wave velocities, which vary from 2.8 to 3.6 km s^{-1}, with an average of 3.3 ± 0.2 km s^{-1}. Poisson's ratios for the whole crust range from 0.26 to 0.31, with values generally increasing with distance from the Precambrian terranes of Madagascar, and an average of 0.29 ± 0.02. The thickness of the mafic layer at the bottom of the crust varies between 3 and 13 km for all of the basin stations, with an average of 4 ± 3 km, and uppermost mantle shear-wave velocities that range from 4.3 to 4.5 km s^{-1}.

4.2 Palaeoarchean to Mesoarchean terrane

The crust beneath the Antongil-Masora craton is 43 km thick, although only one station was located in this terrane. The crust is characterized by an average crustal shear-wave velocity of 3.7 km s^{-1}, a Poisson's ratio of 0.24, and a 15-km-thick mafic lower crust. The average shear-wave velocity of the uppermost mantle here is 4.5 km s^{-1}.

4.3 Neoarchean terrane

The Moho beneath the Antananarivo terrane ranges in depth from 33 to 46 km, with an average depth of 40 km. The crust of the northernmost part of the terrane is the thinnest, with a Moho depth of 33 km. The crust is thicker, with a Moho depth between 41 and 46 km, beneath the central and southern parts of the terrane, and thins to 36 km along the east coast. The average shear-wave velocity of the crust for this region is 3.7 km s^{-1}, the average crustal Poisson's ratio is 0.25, and the average thickness of the mafic lower crust is 6 km. The average shear-wave velocity of the uppermost mantle is 4.4 km s^{-1}.

4.4 Palaeoproterozoic terrane

The crustal thickness beneath the Anosyen-Androyen terrane ranges from 36 to 38 km, with an average of 37 km. The crust is characterized by an average shear-wave velocity of 3.7 km s^{-1}, an average Poisson's ratio of 0.24, and an average thickness of the mafic lower crust of 4 km. The average uppermost mantle shear-wave velocity is 4.5 km s^{-1}.

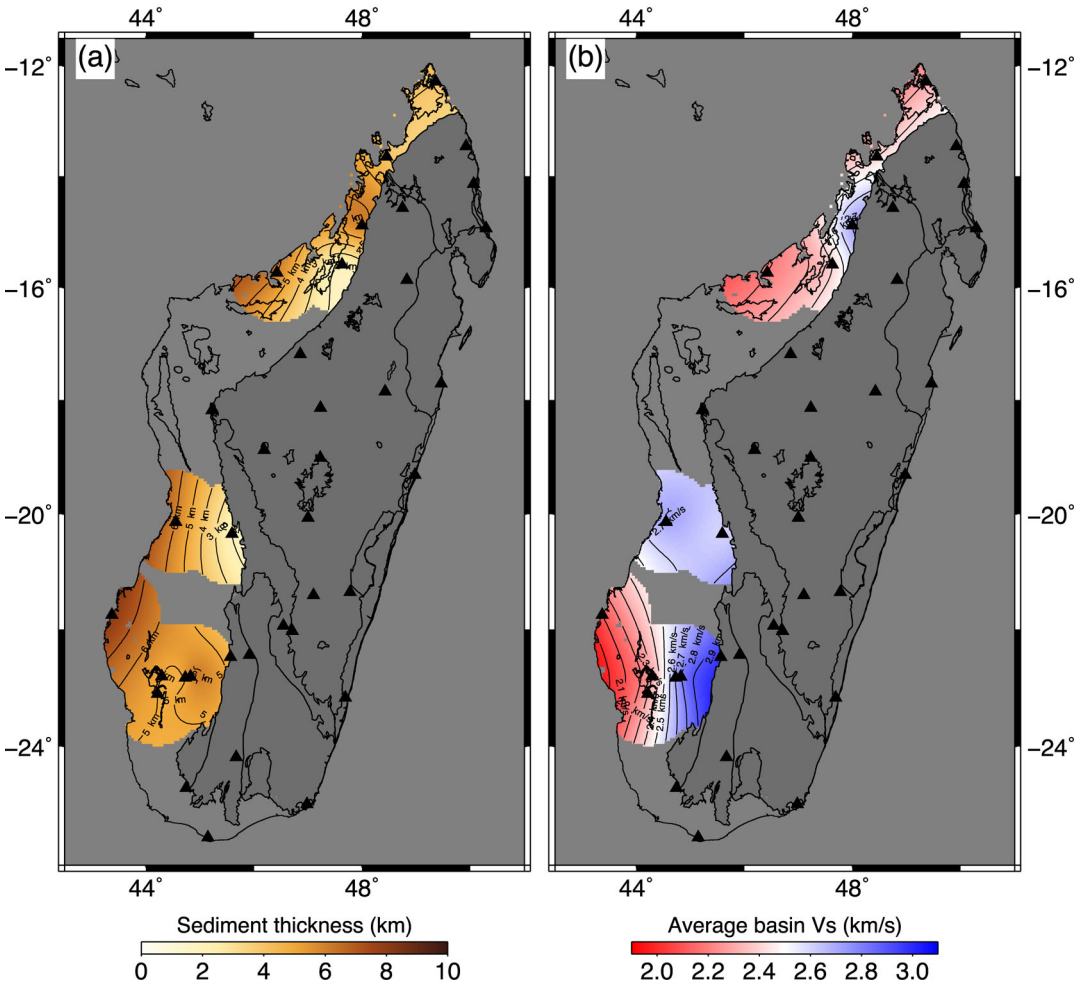

Figure 9. Contour maps of (a) basin thicknesses and (b) average basin shear-wave velocities using seismic stations located in the sedimentary basin. All are interpolated from the point estimates of the station values. Also plotted are the major geological unit boundaries shown in Fig. 1 and station locations (black triangles).

4.5 Mesoproterozoic terrane

The two stations in the Ikalamavony terrane are located far apart and have more in common with other stations near to them than with each other. Station VINA is at the north end of the terrane bordering the sedimentary basin and its crustal thickness of 36 km is similar to the 33-km-thick crust under station BAND. Beneath station MS16, which is located between the Antananarivo and Anosyen-Androyen terranes, the crust is 41 km thick, similar to the thickness of the crust found under station VOI. For both stations the average crustal shear-wave velocity is 3.7 km s^{-1}, Poisson's ratios are 0.23 and 0.24, and the thickness of the mafic lower crust is 5–8 km. The uppermost mantle has shear-wave velocities of 4.4–4.5 km s^{-1}.

4.6 Neoproterozoic terrane

The crustal thicknesses beneath the Bemarivo terrane range from 31 to 36 km, with an average of 33 km. For the Vohibory terrane, the crustal thickness determined from a single station is 28 km. The crust of both terranes is characterized by averaged shear-wave velocities of 3.5–3.7 km s^{-1}. The average Poisson's ratio for both terranes is 0.30. The thickness of the mafic lower crust is 2 km thick on average beneath the Bemarivo terrane and 0 km thick under the Vohibory terrane. The shear-wave velocity of the uppermost mantle under the Bemarivo terrane is 4.2 to 4.3 and 4.4 km s^{-1} under the Vohibory terrane.

5 DISCUSSION

The main findings of this study reflect the complex geological history of the island and are broadly consistent with previous estimates of crustal structure, where such estimates exist. To summarize, sedimentary basin thickness decreases northwards and eastwards. The average crustal shear-wave velocities increase from west to east, mostly as a result of the diminishing effect of thinner sedimentary layers. The crust beneath the high plateau that runs along the central spine of Madagascar is noticeably thicker than most of the peripheral regions. This region correspondingly contains the oldest basement rocks of Madagascar, and is representative of the fact that the crustal thickness and other seismic parameters of different regions of Madagascar are strongly representative of its Palaeogeographic and tectonic history. Results also show variable architecture of the Moho discontinuity, that is sharp or gradational, for the Precambrian terranes of Madagascar.

The thinning of the basins (Fig. 9a), which reflects both the eastward and northward progression in the rifting that formed the basins, has been mentioned previously in several studies, including Besairie (1971), Razafimbelo (1987), Coffin & Rabinowitz (1988)

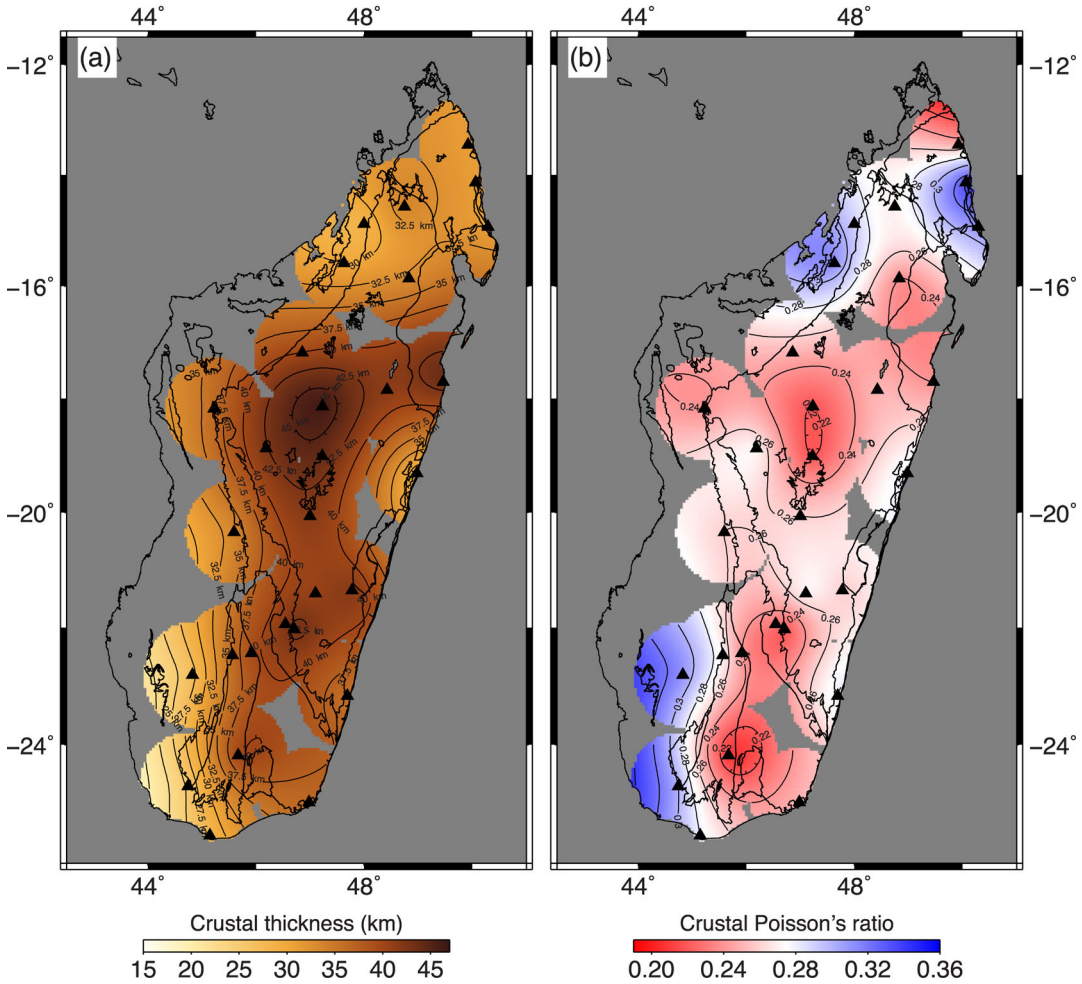

Figure 10. Contour maps of (a) crustal thicknesses and (b) Poisson's ratio using 29 stations from which the H–κ stacking technique was applied. All are interpolated from the point estimates of the station values. Also plotted are the major geological unit boundaries shown in Fig. 1 and station locations (black triangles).

and Piqué (1999b), but is not as well characterized as in this study. In terms of seismic shear-wave velocities, the western parts of the basins are slower, at ∼2.3 km s^{-1}, compared to ∼2.6 km s^{-1} for the eastern parts (Fig. 9b). The higher velocities observed in the eastern parts of the basins can be explained by the fact that the Karoo facies, which are mainly sandstones, outcrop only in the eastern parts of the basin (Wescott & Diggens 1997, 1998), suggesting that the shear-wave velocities in the western part of the basin are influenced by the younger deposits overlying the Karoo sequence.

It is reasonable to assume that before Madagascar rifted away from Africa the thickness of the crust along the western parts of Madagascar was similar to the thickness of unrifted Precambrian crust both to the east, found in this study to be 38 ± 5 km, and in eastern Africa, found by Kachingwe *et al.* (2015) to be 38–39 ± 3 km. Given this, and the thickness of the crust beneath the western rifted margin of Madagascar, the amount of crustal thinning beneath the sedimentary basins can be estimated. In the northernmost part of the island, it thus appears that the crust has been thinned by ∼20 km (i.e. 38 km versus 18 km), and along the west-central and south-central edges of the island, it appears that the crust has been thinned by ∼12 km (i.e. 38 km versus 23–26 km).

The crust on the east coast of Madagascar is also observed to be thinner than in the central highland plateau of the island, but not nearly as thin as beneath the west coast (Figs 10a and 11a). With the exception of station ANLA (in the Palaeoarchean Antongil craton), the east-coast stations of SBV, MKVA, LAHA, MAGY, MAHA and FOMA display crustal thicknesses that are similar, with an average thickness of 34 km. The differences in crustal structure between the east and west coasts can be understood from the different ways in which breakup was accommodated. Along the east coast, India moved northward along what was primarily a transform fault, so there was not the same development of extensional basins as found along the west side of the island.

The separation of India from Madagascar was likely influenced by the passage of the Greater India block over the Marion hotspot about 95–85 Ma, when the extensive floods basalts covered much of the island (Storey *et al.* 1995; Torsvik *et al.* 1998). The thermal anomaly associated with the hotspot likely weakened and thinned Madagascar's lithosphere, facilitating the break-away of the Greater India block along the edge of the Western Dharwar Craton (Raval & Veeraswamy 2003). The slight thinning of the crust found along the east coast of Madagascar could be the result of uplifting and erosion of the crust due to the Marion plume, as opposed to or in addition to a minimal component of rifting.

In contrast to our findings, Paul & Eakin (2017) concluded that the crust beneath the central region of Madagascar is thinner compared to the eastern coast based on the analysis of records from the permanent stations ABPO in central Madagascar, and FOMA

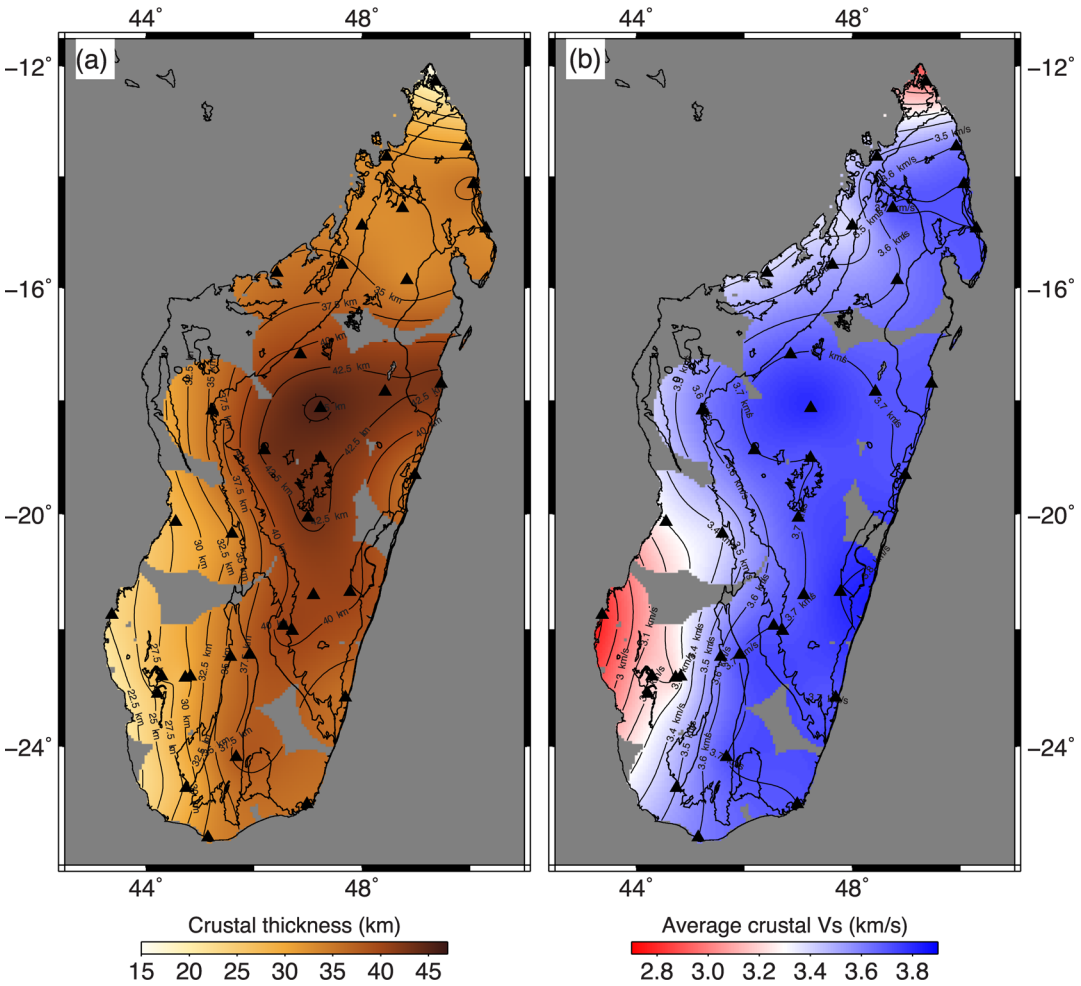

Figure 11. Contour maps of (a) crustal thicknesses and (b) average crustal shear-wave velocities using 37 stations from which the joint receiver function inversion method was applied. All are interpolated from the point estimates of the station values. Also plotted are the major geological unit boundaries shown in Fig. 1 and station locations (black triangles).

along the southern coast. The main discrepancy arises for FOMA, where their estimate of 44 km contrasts with our estimate of 36 km. Their high estimate is clearly due to their interpretation of a phase in the receiver functions, at ∼6 s, as the direct Ps conversion from the Moho. However, this arrival could also be a multiple of an intra-crustal phase (at ∼2 s; see Fig. S4). Note that Paul & Eakin (2017) only considered teleseismic events with back azimuths between 82° and 93°. However, looking at other backazimuth ranges (Fig. S4, in this study), a clear phase, presumably the Ps wave converted from the Moho discontinuity, is observed at ∼4 s. This indicates thinner crust (∼36 km) as reported in this study and earlier ones using receiver functions (e.g. Rindraharisaona *et al*. 2013, 2017), which used more than one station along the eastern coast and considered broader back azimuth ranges. In support of this interpretation, crustal thickness estimates from gravimetry imply that the crust thins towards the eastern coast (Fourno & Roussel 1994; Rakotondraompiana *et al.* 1999). Therefore, the balance of evidence points to the shallower Moho inferred in our joint inversion but the presence of the strong phase at 6 s for azimuths between ∼60° and 130° points to lateral variability, which is beyond the scope of the current study to investigate further.

Several studies have investigated variations in crustal structure with age in order to assess secular variation in the continental crust. Some studies have reported that Archean crust is thinner than Proterozoic crust (e.g. Durrheim & Mooney 1991, 1994; Thompson *et al.* 2010), while others have found little evidence for age-dependent differences (e.g. Rudnick & Fountain 1995; Zandt & Ammon 1995; Tugume *et al*. 2012, 2013; Kachingwe *et al.* 2015). Crustal thicknesses obtained in this study suggest that the Archean crust (40 ± 4 km) in Madagascar is on average slightly thicker than the Proterozoic crust (35 ± 4 km). In contrast, there are no significant differences in Poisson's ratio between the Archean crust (0.25 ± 0.02) and Proterozoic crust (0.26 ± 0.04) or in average shear wave velocities (3.7 km s^{-1} for both), though the average thickness of the mafic lower crust is slightly greater for Archean terranes (7 km) than it is for Proterozoic terranes (4 km). Our results are in broad agreement with Rindraharisaona *et al.* (2017). They concluded that the Archean crust is also slightly thicker (38–43 km) compared to the Proterozoic crust (33–38 km). They attributed the difference to the absence of a mafic lower crustal underplate in the Proterozoic terranes, and suggested that the underplated layer may have delaminated due to the high-temperature metamorphism that affected the areas, a process described by Martelat *et al.* (2000); Jöns & Schenk (2011), and Horton *et al.* (2016).

The observed variations in the crustal Poisson's ratio can be interpreted as the result of changes in silicic compositions. Laboratory measurements (e.g. Christensen 1996) have demonstrated that Poisson's ratio is 0.24 for felsic granitic rocks, 0.27 for

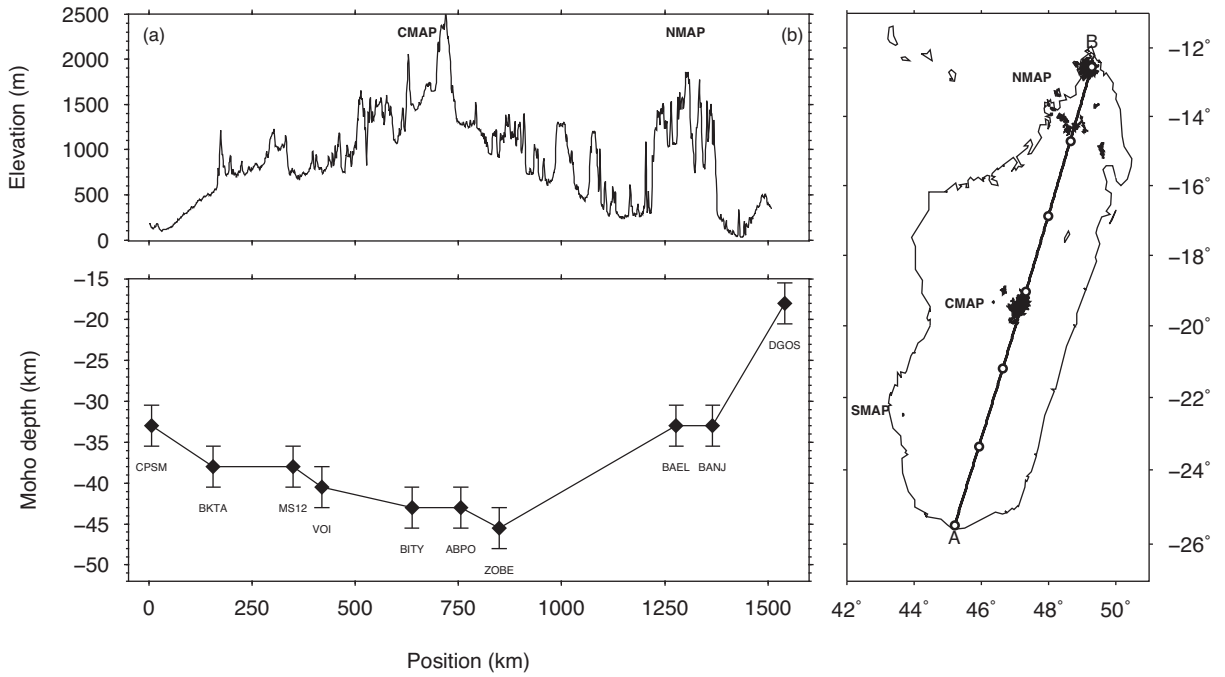

Figure 12. Top panel: elevation of Madagascar (Amante & Eakins 2009) along the profile A–B. The Cenozoic volcanic provinces NMAP and CMAP are shown in the figure at right (in black). Bottom panel: crustal thickness values for seismic stations along the same profile. Right-hand panel: white circles along the profile are 250 km intervals from the 0 km position at A.

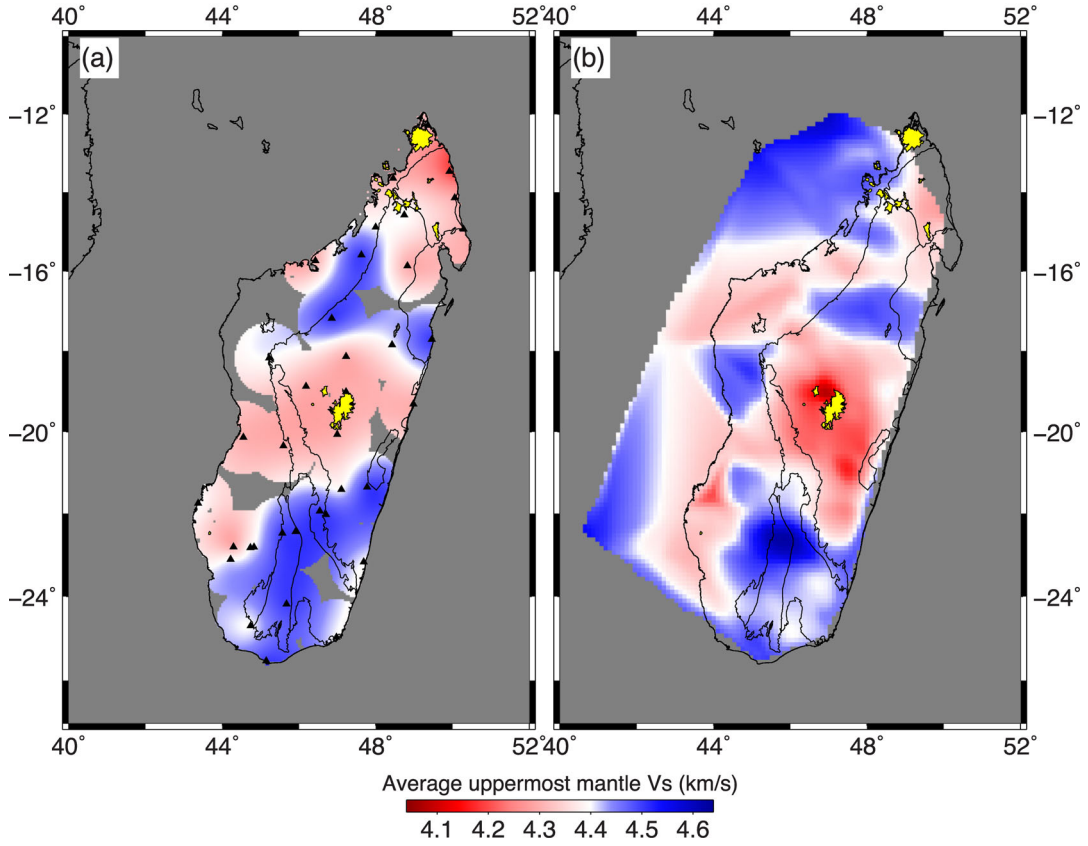

Figure 13. Maps showing (a) the average uppermost mantle shear-wave velocities, interpolated from the point estimates of the station values from this study and (b) the shear velocities at 50 km depth from the surface-wave tomography in Pratt *et al.* (2017). Also plotted are the major geological unit boundaries shown in Fig. 1, the locations of the NMAP/CMAP/SMAP provinces (Northern, Central and Southern Madagascar Alkaline Provinces, respectively) (in yellow), and station locations (black triangles). The regions where the uppermost mantle shear-wave velocities are anomalously low correspond very well with regions of Cenozoic volcanic activity and with low-velocity mantle anomalies determined from the surface-wave study of Pratt *et al.* (2017).

intermediate lithologies (such as diorite), and 0.30 for mafic gabbros. We found the Archean and Proterozoic terranes to have a Poisson's ratio that ranged from 0.2 to 0.3 with, an average of 0.26 ± 0.03 (Fig. 10b). Overall, the crust of these terranes is representative of predominantly felsic to intermediate compositions. In contrast, the eastern regions of the west-coast sedimentary basins have higher crustal Poisson's ratio of 0.29 ± 0.02. It is possible that this reflects the syntectonic emplacement of rift basalts while the Greater India block was rifting away from Africa, as has been found at other large continental rifts (Stein *et al.* 2016), imparting a slightly more mafic composition to the crust. However, this interpretation is not supported by the low average crustal shear-wave velocities (3.3 km s^{-1}) or the thin mafic lower crust (4 km) under the basins. An alternative and maybe more likely possibility is that the higher Poisson's ratio results simply from the contribution of the sediments in the basin, which can have a higher Poisson's ratio than crystalline rocks.

As can be seen in Fig. 12, which shows a N–S profile across the length of Madagascar, there is a very strong correlation between elevation and crustal thickness. An increase from 33 to 46 km is observed for the crustal thickness of Madagascar, compared to a corresponding variation of 0–1.6 km in elevation at the surface. A comparison of the two curves reveals a change in Moho depth that is approximately eight times greater than the corresponding change in surface relief, suggesting that it can be fairly well explained by an Airy model of isostatic equilibrium.

However, this correlation breaks down in the northern part of the island, where elevations range from 1 to 2 km but crustal thicknesses are less than 35 km. Given that Madagascar has not undergone any tectonic activity in the past 85 Myr, some other mechanism is required to maintain this high elevation. One possibility is that the northern region is dynamically supported by the same thermal anomalies that have been the source of late Cenozoic volcanism in the north. In general, the pattern of isostatic equilibrium suggested by Fig. 12 is superimposed upon a broad signature of uplift for the island. The average crustal thickness across all stations is 35 km while the average elevation of the stations is 496 m. This elevation is unusually high for the slightly thinner-than-average crustal thickness, suggesting that an additional factor is needed to explain the high elevations. It is likely that the three large regions of seismically slow velocities in the upper mantle beneath the northern, central, and southwestern regions of Madagascar, imaged by Pratt *et al.* (2017; Fig. 13), correspond to thermal anomalies that provide the buoyancy needed to maintain these high elevations. This is supported by observations of the erosion rates of river valleys and lavakas (erosional gullies), which suggest that Madagascar has been experiencing active uplift for at least the past 15 Myr (Cox *et al.* 2010; Roberts *et al.* 2012).

The uppermost mantle beneath Madagascar is generally characterized by average shear-wave velocities that range from 4.2 to 4.5 km s^{-1}, with an overall average of 4.4 ± 0.1 km s^{-1} (Fig. 13). The shear velocity of the uppermost mantle drops to values of 4.2–4.3 km s^{-1} in the northern part (beneath seismic stations DGOS, BANJ, SBV, MKVA and LAHA), central part (beneath stations ZOBE, ABPO, BATG, BITY and MAGY), and western and southwestern parts (beneath stations MAJA, BAND, KIRI and LONA). These slow mantle velocities of 4.2–4.3 km s^{-1} coincide with the three major volcanic provinces in Madagascar (NMAP, CMAP and SMAP) that are observed to have upper mantle low-shear-velocity anomalies from surface wave tomography (Pratt *et al.* 2017; see Figs 13a and b). The anomalies in the northern and central parts correspond to locations of Cenozoic volcanic activity within the past 1 Ma (Tucker & Conrad 2008), while the slow upper mantle *Vs* in the western, southwestern, and eastern parts correspond to Cretaceous surface volcanism, and also 9-Ma-old volcanics in the southwestern region of Ankililoaka (Bardintzeff *et al.* 2010).

6 CONCLUSIONS

The seismic structure of the crust and uppermost mantle of Madagascar has been investigated using broadband data recorded on 37 temporary and permanent broad-band seismic stations. We applied the H–κ stacking procedure to seismic stations deployed on the Precambrian basement and the easternmost parts of the sedimentary basins to calculate the crustal thickness (H) and bulk crustal Vp/Vs ratio (κ), from which Poisson's ratio was determined. Receiver functions were jointly inverted with Rayleigh-wave phase-velocity dispersion measurements to image the Moho and obtain vertical profiles of shear-wave velocities.

Our results reveal that basins along the west coast thin both eastward, from depths of 6–8 to 2 km, and northward, from depths of 5–8 to 4 km, reflecting the eastwardly and northwardly progressive opening and filling of the sedimentary basins. The thickness of Madagascar's crust ranges between 18 and 46 km. Beneath the western basins the crust is thinner (18–36 km thick) because of the Mesozoic rifting of Madagascar from eastern Africa. In comparison to estimates of the thickness of nearby unrifted crust, it appears that the rifted crust has been vertically thinned by as much as ∼12 to 20 km.

There is a weak evidence for secular variation in the structure of the Precambrian crust in Madagascar. The Archean terranes have an average crustal thickness of 40 km and average Poisson's ratio of 0.25, and the Proterozoic terranes have an average crustal thickness of 35 km and average Poisson's ratio of 0.26. The thickness of the mafic lower crust is great for Archean terranes (7 km) than for Proterozoic terranes (4 km), but both have similar average crustal shear-wave velocities (3.7 km s^{-1}).

Crustal thickness beneath the Precambrian terranes along the east coast of Madagascar ranges from 31 to 36 km, somewhat thinner than beneath the interior of the island. The small amount of thinning may have been caused by crustal uplift and erosion when Madagascar moved over the Marion hotspot and India broke away.

The uppermost mantle beneath Madagascar is generally characterized by average shear-wave velocities that range from 4.2 to 4.5 km s^{-1}, with an overall average of 4.4 ± 0.1 km s^{-1}. The shear-wave velocity of the uppermost mantle drops to values of 4.2–4.3 km s^{-1} in the northern, central, and southern parts of the island, coincident with the three major volcanic provinces in Madagascar.

There is a fairly good correlation between station elevation and the underlying crustal thickness across Madagascar, with about a 1 km change in elevation at the surface of Madagascar corresponding to a change of 8 km in Moho topography. However, in the northern part of the island, surface elevations are anomalously high compared to crustal thicknesses, suggesting a source of dynamic topography that might be provided by an upper mantle thermal anomaly that would also explain the slow uppermost mantle shear-wave velocities of 4.2–4.3 km s^{-1} and episodes of recent volcanic activity.

ACKNOWLEDGEMENTS

We gratefully acknowledge the field support from IRIS-PASSCAL, which provided the seismic equipment for the MACOMO project (FDSN code: XV 2011–2013, Wysession *et al.* 2011);

SELASOMA project (FDSN code: ZE2012–2014, Tilmann *et al.* 2012), IRIS (FDSN code: II, Scripps Institution of Oceanography 1986), AFRICAARRAY (FDSN code: AF, Penn State University 2004), GEOFON (FDSN code: GE, GEOFON Data Centre 1993) and GEOSCOPE (FDSN code: G, Institut de Physique du Globe de Paris (IPGP) & Ecole et Observatoire des Sciences de la Terre de Strasbourg (EOST) 1982) for additional seismic data. Figures in this paper have been produced with GMT (Wessel & Smith 1998). This research was funded by the National Science Foundation, through grants EAR-0838426 and 0838387. We thank E. Rindraharisaona for her constructive comments and discussion. We also thank an anonymous reviewer and Stewart Fishwick for providing insightful reviews which helped to improve the paper.

REFERENCES

Amante, C. & Eakins, B.W., 2009. ETOPO1 1 arc-minute global relief model: procedures, data sources and analysis, NOAA Technical Memorandum NESDIS NGDC-24, National Geophysical Data Center, NOAA. doi:10.7289/V5C8276M.

Ammon, C.J., Randall, G.E. & Zandt, G., 1990. On the nonuniqueness of receiver function inversions, *J. geophys. Res.,* **95,** 15 303–15 318.

Bardintzeff, J-M., Liegeois, J-P., Bonin, B., Bellon, H. & Rasamimanana, G., 2010. Madagascar volcanic provinces linked to the Gondwana breakup: geochemical and isotopic evidences for contrasting mantle sources, *Gondwana Res.,* **18,** 295–314.

Berteussen, K.A., 1977. Moho depth determinations based on spectral ratio analysis of NORSAR long-period P waves, *Phys. Earth planet. Int.,* **31,** 313–326.

Besairie, H., 1968. Description géologique du massif ancien de Madagascar, Premier volume: Centre Nord et Centre Nord-Est, Doc. Bur. Geol. n°177a, Service Géologique, Antananarivo. Ministère de l'Industrie et des Mines, Direction des Mines et de l'Energie, 117 pp.

Besairie, H., 1969. Description géologique du massif ancien de Madagascar, Deuxième volume: La regioncotière orientale entre le Mangoro et Vangaindrano. Doc. Bur. Geol. n°177b, Service Géologique, Antananarivo. Ministère de l'Industrie et des Mines, Direction des Mines et de l'Energie, 67 pp.

Besairie, H., 1971. Tectonique de madagascar. Tectonique de l' Afrique. *Sciences de la Terre UNESCO Paris,* 549–558.

Besairie, H., 1973. Brève revue de volcanisme à Madagascar. Colloque sur les régions volcaniques tropicales, *Pub. Ass. Géogr., Madagascar,* 18 pp.

Boast, J. & Nairn, A.E.M., 1982. An outline of the geology of Madagascar, in *The Ocean Basins and Margins,* pp. 649–696, eds Nairn, A.E.M. & Stehli, F.G., Plenum Press.

Brocher, T.A., 2005. Empirical relations between elastic wavespeeds and density in the Earth's crust, *Bull. seism. Soc. Am.,* **95,** 2081–2092.

Cassidy, J.F., 1992. Numerical experiments in broadband receiver function analysis, *Bull. seism. Soc. Am.,* **82,** 1453–1474.

Castagna, J.P., Batzle, M.L. & Eastwood, R.L., 1985. Relationships between compressional-wave and shear-wave velocities in clastic silicate rocks, *Geophysics,* **50,** 571–581.

Christensen, N.I., 1996. Poisson's ratio and crustal seismology, *J. geophys. Res.,* **101,** 3139–3156.

Christensen, N.I. & Mooney, W.D., 1995. Seismic velocity structure and composition of the continental crust: a global view, *J. geophys. Res.,* **100,** 9761–9788.

Cochran, J.R., 1988. Somali Basin, Chain Ridge and the origin of the Northern Somali Basin gravity and geoid low, *J. geophys. Res.,* **93,** 11 985–12 008.

Coffin, M.F. & Rabinowitz, P.D., 1987. Reconstruction of Madagascar and Africa: evidence from the Davie fracture zone and Western Somali Basin, *Geophys. Res. Lett.,* **92,** 9385–9406.

Coffin, M.F. & Rabinowitz, P.D., 1988. Evolution of the conjugate East African-Madagascan margins and the western Somali Basin, *Spec. Pap. Geol. Soc. Am.,* **226,** 78.

Collins, A.S., 2006. Madagascar and the amalgamation of Central Gondwana, *Gondwana Res*., **9,** 3–16.

Cox, R., Coleman, D.S., Chokel, C.B., DeOreo, S.B., Wooden, J.L., Collins, A.S., Kröner, A. & DeWaele, B., 2004. Proterozoic tectonostratigraphy and paleogeography of central Madagascar derived from detrital zircon U-Pb age populations, *J. Geol.,* **112,** 379–399.

Cox, R., Zentner, D.B., Rakotondrazafy, A.M. & Rasoazanamparany, C.F., 2010. Shakedown in Madagascar: occurrence of lavakas (erosional gullies) associated with seismic activity, *Geology,* **38,** 179–182.

de Wit, M.J., 2003. Madagascar: heads it's a continent, tails it's an island, *Ann. Rev. Earth planet. Sci,* **31,** 213–248.

Durrheim, R.J. & Mooney, W.D., 1991. Archean and Proterozoic crustal evolution: evidence from crustal seismology, *Geology,* **19,** 606–609.

Durrheim, R.J. & Mooney, W.D., 1994. Evolution of the Precambrian lithosphere: seismological and geochemical constraints, *J. geophys. Res.,* **99,** 15 359–15 374.

Dyment, J., 1991. Structure et évolution de la lithosphère océanique dans l'Océan Indien: apport des données magnétiques, *PhD thesis*, Univ. Strasbourg, 374 pp.

Dziewonski, A.M. & Anderson, D.L., 1981. Preliminary reference earth model, *Phys. Earth planet. Inter.,* **25,** 297–356.

Efron, B. & Tibshirani, R., 1991. Statistical data analysis in computer age, *Science,* **253,** 390–395.

Fourno, J.P. & Roussel, J., 1994. Imaging of the Moho depth in Madagascar through the inversion of gravity data: geodynamic implications, *Terra Nova,* **6,** 512–519.

GAF-BGR, 2008. Final report. Explanatory notes for the Vohibory Domain southwest Madagascar. Réalisation des travaux de cartographie géologique de Madagascar, révision approfondie de la cartographie géologique et minière aux échelles 1/100000 et 1/500000 zone Sud. République de Madagascar, Ministère de L'Energie et des Mines (MEM/SG/DG/UCP/PGRM), 85 pp.

Holbrook, W.S., Mooney, W.D. & Christensen, N.I., 1992. The seismic velocity structure of the deep continental crust, in *Continental Lower Crust,* chapt. 1, pp. 1–43, eds Fountain, D.M., Arculus, R. & Kay, R.W., Elsevier.

Horton, F., Hacker, B., Kylander-Clark, A., Holder, R. & Jöns, N., 2016. Focused radiogenic heating of middle crust caused ultrahigh temperatures in southern Madagascar, *Tectonics,* **35,** 293–314.

Hottin, G., 1976. Présentation et essai d'interprétation du Précambrien de Madagascar, *Bulletin du Bureau de Recherches Géologiques et Minières,* 2nd série, Vol. IV, 117–153.

Institut de Physique du Globe de Paris (IPGP), & Ecole et Observatoire des Sciences de la Terre de Strasbourg (EOST)., 1982. GEOSCOPE, French Global Network of broad band seismic stations, Institut de Physique du Globe de Paris (IPGP), https://doi.org/10.18715/GEOSCOPE.G.

Jöns, N. & Schenk, V., 2008. Relics of the Mozambique Ocean in the central East African Orogen: evidence from the Vohibory Block of southern Madagascar, *J. Metamorph. Geol.,* **26,** 17–28.

Jöns, N. & Schenk, V., 2011. The ultrahigh temperature granulites of southern Madagascar in a polymetamorphic context: Implications for the amalgamation of the Gondwana supercontinent, *Eur. J. Mineral.,* **23,** 127–156.

Julià, J., 2007. Constraining velocity and density contrasts across the crust-mantle boundary with receiver function amplitudes, *Geophys. J. Int.,* **171,** 286–301.

Julià, J. & Mejía, J., 2004. Thickness and *Vp*/*Vs* ratio variation in the Iberian crust, *Geophys. J. Int.,* **156,** 59–72.

Julià, J., Ammon, C.J. & Herrmann, R.B., 2003. Lithospheric structure of the Arabian Shield from the joint inversion of receiver functions and surface-wave group velocities, *Tectonophysics,* **371,** 1–21.

Julià, J., Ammon, C.J. & Nyblade, A.A., 2005. Evidence for mafic lower crust in Tanzania, East Africa, from joint inversion of receiver functions and Rayleigh wave dispersion velocities, *Geophys. J. Int.,* **162,** 555–562.

Julià, J., Assumpção, M. & Rocha, M.P., 2008. Deep crustal structure of the Paranã Basin from receiver functions and Rayleigh-wave dispersion: evidence for a fragmented cratonic root, *J. geophys. Res.,* **113,** B08318. doi:10.1029/2007JB005374.

Julià, J., Ammon, C.J., Herrmann, R.B. & Correig, A.M., 2000. Joint inversion of receiver function and surface wave dispersion observations, *Geophys. J. Int.,* **143,** 99–112.

Kachingwe, M., Nyblade, A.A. & Julià, J., 2015. Crustal structure of Precambrian terranes in the southern African subcontinent with implications for secular variation in crustal genesis, *Geophys. J. Int.,* **202,** 533–547.

Langston, C.A., 1979. Structure under Mount Rainier, Washington, inferred from teleseismic body waves, *J. geophys. Res.,* **84,** 4749–4762.

Laske, G., Masters, G., Ma, Z. & Pasyanos, M., 2013. Update on CRUST1.0 - A 1-degree Global Model of Earth's Crust, *Geophys. Res. Abstr.,* **15,** Abstract EGU2013-2658.

Ligorría, J.P. & Ammon, C.J., 1999. Iterative deconvolution and receiver function estimation, *Bull. seism. Soc. Am.,* **89,** 1395–1400.

Mahoney, J., Nicollet, C. & Dupuy, C., 1991. Madagascar basalts: tracking oceanic and continental sources, *Earth planet. Sci. Lett.,* **104,** 350–363.

Martelat, J.-E., Lardeaux, J.-M., Nicollet, C. & Rakotondrazafy, R., 2000. Strain pattern and late Precambrian deformation history in southern Madagascar, *Precambrian Res*., **102,** 1–20.

Nicollet, C., 1990. Crustal evolution of the granulites of Madagascar, in: *Granulites and Crustal Evolution*, pp. 291–310, eds Vielzeuf, D. & Vidal, P.H.

Norton, I.O. & Sclater, J.G., 1979. A model for the evolution of the Indian Ocean and the breakup of Gondwanaland, *J. geophys. Res.,* **84,** 6803–6830.

Owens, T.J., Zandt, G. & Taylor, S.R., 1984. Seismic evidence for an ancient rift beneath the Cumberland Plateau, Tennessee; a detailed analysis of broadband teleseismic P-waveforms, *J. geophys. Res.,* **89,** 7783–7795.

Pasyanos, M.E. & Nyblade, A.A., 2007. A top to bottom lithospheric study of Africa and Arabia, *Tectonophysics,* **444,** 27–44.

Paul, J.D. & Eakin, C.M., 2017. Mantle upwelling beneath Madagascar: evidence from receiver function analysis and shear wave splitting, *J. Seismol,* 1–12.

Penn State University, 2004. AfricaArray. International Federation of Digital Seismograph Networks, *Other/Seismic Network*. doi:10.7914/SN/AF.

Piqué, A., 1999a. The geological evolution of Madagascar: an introduction, *J. Afr. Earth Sci.,* **28,** 919–930.

Piqué, A., 1999b. The initiation and development of the Morondava Basin (Madagascar) from the Late Carboniferous to the Middle Jurassic: sedimentary, palaeontological and structural data, *J. Afr. Earth Sci.,* **28,** 931–948.

Pratt, M.J. *et al.*, 2017. Shear-velocity structure of the crust and upper mantle of Madagascar derived from surface wave tomography, *Earth planet. Sci. Lett.,* **458,** 405–417.

Rabinowitz, P.D., Coffin, M.F. & Falvey, D., 1983. The separation of Madagascar and Africa, *Science,* **220,** 67–69.

Rai, A., Gaur, V.K., Rai, S.S. & Priestley, K., 2009. Seismic signatures of the Pan African orogeny: implications for southern Indian high grade terranes, *Geophys. J. Int.,* **176,** 518–528.

Rajaomazava, F., 1992. Etude de la subsidence du bassin sédimentaire de Morondava (Madagascar) dans le cadre de l'évolution géodynamique de la marge Est-Africaine, *PhD thesis*, Univ. Montpellier, France.

Rakotondrainibe, 1977. Contribution à l'étude de la séismicité de Madagascar, *PhD Thesis*, Univ. Antananarivo, Madagascar.

Rakotondraompiana, S.A., Albouy, Y. & Piqué, A., 1999. Lithospheric model of the Madagascar island (western Indian Ocean): a new interpretation of the gravity data, *J. Afr. Earth Sci.,* **28,** 961–973.

Rambolamanana, G., Suhadolc, P. & Panza, G.F., 1997. Simultaneous inversion of hypocentral parameters and structure velocity of the central region of Madagascar as a premise for the mitigation of seismic hazard in Antananarivo, *Pure appl. Geophys.,* **149,** 707–730.

Raval, U. & Veeraswamy, K., 2003. India-Madagascar separation: breakup along a pre-existing mobile belt and chipping of the craton, *Gondwana Res.,* **6,** 467–485.

Razafimbelo, M.E., 1987. Le bassin de Morondava (Madagascar) synthèse géologique et structurale, *PhD thesis*, Univ. Louis-Pasteur, France.

Reiss, M.C., Rümpker, G., Tilmann, F., Yuan, X., Giese, J. & Rindraharisaona, E.J., 2016. Seismic anisotropy of the lithosphere and asthenosphere beneath southern Madagascar from teleseismic shear wave splitting analysis and waveform modeling, *J. geophys. Res.,* **121,** doi:10.1002/2016JB013020.

Rindraharisaona, E.J., Guidarelli, M., Aoudia, A. & Rambolamanana, G., 2013. Earth structure and instrumental seismicity of Madagascar: implications on the seismotectonics, *Tectonophysics,* **594,** 165–181.

Rindraharisaona, E.J., Tilmann, F., Yuan, X., Rümper, G., Giese, J., Rambolamanana, G. & Barruol, G., 2017. Crustal structure of southern Madagascar from receiver functions and ambient noise correlation: implications for crustal evolution, *J. geophys. Res.,* **122**(2), 1179–1197.

Roberts, G.G., Paul, J.D., White, N. & Winterbourne, J., 2012. Temporal and spatial evolution of dynamic support from river profiles: a framework for Madagascar, *Geochem. Geophys. Geosyst.,* **13,** Q04004, doi:10.1029/2012GC004040.

Rudnick, R.L. & Fountain, D.M., 1995. Nature and composition of the continental crust the continental crust: a lower crustal perspective, *Rev. Geophys.,* **33,** 267–309.

Rudnick, R.L. & Gao, S., 2003. Composition of the continental crust, in *Treatise on Geochemistry*, Vol. 3, Elsevier, 64 pp.

Schlich, R., 1975. Structure et âge de l'océan Indien occidental, *Mem. Soc. Geol. Fr.,* **6,** 102.

Scripps Institution of Oceanography, 1986. IRIS/IDA Seismic Network. International Federation of Digital Seismograph Networks. Other/Seismic Network. doi:10.7914/SN/II.

Segoufin, J. & Patriat, P., 1980. Existence d'anomalies mésozoïques dans le bassin de Somalie. Implications pour les relations Afrique-Antarctique-Madagascar, *C.R. Acad. Sci.,* Paris, **291,** 85–88.

Stein, S. *et al.*, 2016. New insights into North America's Midcontinent Rift, *Eos,* **97,** doi:10.1029/2016EO056659.

Stein, S. & Wysession, M., 2003. *An Introduction to Seismology, Earthquakes and Earth Structure,* Blackwell, Malden, MA.

Storey, M., Mahoney, J.J., Saunders, A.D., Duncan, R.A., Kelley, S.P. & Coffin, M.F., 1995. Timing of hotspot related volcanism and breakup of Madagascar and India, *Science,* **267,** 852–855.

Tedla, G.E, Van der Meijde, M., Nyblade, A.A. & Van der Meer, F.D., 2011. A crustal thickness map of Africa derived from a global gravity field model using Euler deconvolution, *Geophys. J. Int.,* **187,** 1–9.

Thomas, R.J. *et al.*, 2009. Geological evolution of the Neoproterozoic Bemarivo Belt, northern Madagascar, *Precambrian Res.,* **172,** 279–300.

Thompson, D.A., Bastow, I.D., Helffrich, G., Kendall, J.M., Wookey, J., Snyder, D.B. & Eaton, D.W., 2010. Precambrian crustal evolution: seismic constraints from the Canadian Shield, *Earth Planet. Sci. Lett.,* **297,** 655–666.

Tilmann, F., Yuan, X., Rümpker, G. & Rindraharisaona, E., 2012. SELASOMA Project, Madagascar 2012–2014, DeutschesGeoForschungsZentrum GFZ, Seismic Network, doi:10.14470/MR7567431421.

Torsvik, T.H., Tucker, R.D., Ashwal, L.D., Eide, E.A., Rakotosolofo, N.A. & de Wit, M.J., 1998. Late Cretaceous magmatism in Madagascar: paleomagnetic evidence for a stationary Marion hotspot, *Earth Planet. Sci. Lett.,* **64,** 221–232.

Tucker, R.D. & Conrad, J., 2008. 40Ar/39Ar geochronology of Mesozoic and younger igneous rocks of central and northern Madagascar, in *Final Report of the BGS-USGS Consortium to the Government of Madagascar,* World Bank Project UK-04-0100, Chapter 7.

Tucker, R.D., Kusky, T.M., Buchwaldt, R. & Handke, M.J., 2007. Neoproterozoic nappes and superposed folding of the Itremo Group, west-central Madagascar, *Gondwana Res.,* **12,** 356–379.

Tucker, R.D., Peters, S.G., Roig, J.Y., Théveniaut, H. & Delor, C., 2012. Notice explicative des cartes géologique et métallogéniques de la République de Madagascar à 1/1000000, Ministère des Mines, PGRM, Antananarivo, République de Madagascar.

Tucker, R.D., Roig, J.Y., Delor, C., Amelin, Y., Goncalves, P., Rabarimanana, M.H., Ralison, A.V. & Belcher, R.W., 2011. Neoproterozoic extension in the Greater Dharwar Craton: a reevaluation of the Betsimisaraka "suture" in Madagascar, *Can. J. Earth Sci.,* **48,** 389–417.

Tugume, F., Nyblade, A. & Julià, J., 2012. Moho depths and Poisson's ratios of Precambrian crust in East Africa: evidence for similarities in Archean

and Proterozoic crustal structure, *Earth Planet. Sci. Lett.,* **355–356,** 73–81.

Tugume, F., Nyblade, A., Julià, J. & van de Meijde, M., 2013. Precambrian crustal structure in Africa and Arabia: evidence lacking for secular variation, *Tectonophysics,* **609,** 250–266.

Wescott, W.A. & Diggens, J.N., 1997. Depositional history and stratigraphical evolution of the Sakoa Group (Lower Karoo Supergroup) in the southern Morondava Basin, Madagascar, *J. Afr. Earth Sci.,* **24,** 585–601.

Wescott, W.A. & Diggens, J.N., 1998. Depositional history and stratigraphical evolution of the Sakamena Group (Middle Karoo Supergroup) in the southern Morondava Basin, Madagascar, *J. Afr. Earth Sci.,* **27,** 461–479.

Wessel, P. & Smith, W.H.F., 1998. New, improved version of Generic Mapping Tools released, *EOS T. Am. Geophys. Un.,* **79,** 579.

Wysession, M., Wiens, D. & Nyblade, A., 2011. Investigation of Sources of Intraplate Volcanism Using PASSCAL Broadband Instruments in Madagascar, the Comores, and Mozambique, International Federation of Digital Seismograph Networks. Other/Seismic Network. doi:10.7914/SN/XV_2011.

Zandt, G. & Ammon, C.J., 1995. Continental crust composition constrained by measurements of crustal Poisson's ratio, *Nature,* **374,** 152–154.

Zhu, L. & Kanamori, H., 2000. Moho depth variation in Southern California from teleseismic receiver functions, *J. geophys. Res.,* **105,** 2969–2980.

SUPPORTING INFORMATION

Supplementary data are available at *GJI* online.

Figure S1. Receiver functions for all stations. The four-column figure shows the radial and tangential calculated from Gaussian parameter 1.0 and 2.5, respectively.

Figure S2. Results from the *H–k* stacking method for all stations. Left-hand panel: H–κ parameter space with the optimal values for H and κ (centre of red ellipse). The black contours map out the percentage values, in the colour scale bar, of the normalized objective function given in eq. (1). Right-hand panel: receiver functions labelled by the event backazimuth (top number) and epicentral distance (bottom number), both in degrees. The optimal results for H and κ obtained are summarized along the top, along with their formal uncertainties, and shown with the red contour on the left-hand panel.

Figure S3. Results from the joint inversion of receiver functions and Rayleigh wave phase-velocity dispersion. Top left-hand panel: grey and black lines are the observed and predicted radial receiver functions, respectively, estimated for Gaussian filter widths of 1.0 (top panel) and 2.5 Hz (bottom panel). The numbers on top of the waveforms are the number of receiver functions stacked (in the square bracket), the average back azimuth (±1 standard deviation), and the average ray parameter (±1 standard deviation) for the stack. Bottom left-hand panel: the observed and predicted dispersion curves of the phase velocity, shown with grey dots and a black line, respectively. Right-hand panel: the starting velocity model (grey line) and predicted velocity structure (black line). The horizontal dash–dotted line and number indicate the Moho depth (in km). The vertical dashed and dotted lines correspond to *Vs* values of 4.0 and 4.3 km s^{-1}.

Figure S4. Receiver functions used (a) in this study and (b) in Paul & Eakin (2017) for the station FOMA. Both figures show Ps conversions at ∼2, ∼4 and ∼6 s. The Ps conversion at ∼2 s likely presents an intracrustal discontinuity. The one at ∼4 s is interpreted as the Moho Ps conversion in this study, which suggests a shallower Moho (∼36 km) than reported in Paul & Eakin (2017). The Ps conversion at ∼6 s was interpreted as the Moho Ps by Paul & Eakin (2017) and yielded a deeper Moho. Note that the arrival at ∼6 s is only strong for northeastern and eastern azimuths.

Table S1. List of seismic stations used in this study.

Table S2. List of seismic events used in this study.

Please note: Oxford University Press is not responsible for the content or functionality of any supporting materials supplied by the authors. Any queries (other than missing material) should be directed to the corresponding author for the paper.